

Parallel Training in Spiking Neural Networks

Yanbin Huang^{a,b}, Man Yao^a, Yuqi Pan^a, Changze Lv^c, Siyuan Xu^a, Xiaoqing Zheng^c, Bo Xu^a, Guoqi Li^{a,*}

^a*Institute of Automation, Chinese Academy of Sciences, Beijing, China*

^b*School of Future Technology, University of Chinese Academy of Sciences, Beijing, China*

^c*School of Computer Science, Fudan University, Shanghai, China*

Abstract

The bio-inspired integrate–fire–reset mechanism of spiking neurons constitutes the foundation for efficient processing in Spiking Neural Networks (SNNs). Recent progress in large models demands that spiking neurons support highly parallel computation to scale efficiently on modern GPUs. This work proposes a novel functional perspective that provides general guidance for designing parallel spiking neurons. We argue that the reset mechanism, which induces complex temporal dependencies and hinders parallel training, should be removed. However, any such modification should satisfy two principles: i) preserving the functions of reset as a core biological mechanism; and ii) enabling parallel training without sacrificing the serial inference ability of spiking neurons, which underpins their efficiency at test time. To this end, we identify the functions of the reset and analyze how to reconcile parallel training with serial inference, upon which we propose a dynamic decay spiking neuron. We conduct comprehensive testing of our method in terms of: i) Training efficiency and extrapolation capability. On 16k-length sequences, we achieve a $25.6 \times$ training speedup over the pioneering parallel spiking neuron [1], and our models trained on 2k-length can stably perform inference on sequences as long as 30k. ii) Generality. We demonstrate the consistent effectiveness of the proposed method across five task categories (image classification, neuromorphic event processing, time-series forecasting, language modeling, and reinforcement learning), three network architectures (spiking CNN/Transformer/SSMs), and two spike activation modes (spike/integer

*Corresponding author

Email addresses: huangyanbin2023@ia.ac.cn (Yanbin Huang), guoqi.li@ia.ac.cn (Guoqi Li)

activation). iii) Energy consumption. The spiking firing of our neuron is lower than that of vanilla and existing parallel spiking neurons.

Keywords: Brain-inspired Computing, Neuromorphic Computing, Spiking Neural Networks, Parallel Training, Efficient Training, Spiking Neuron

1. Introduction

Spiking neurons incorporate information across spatial and temporal domains into a membrane potential, i.e., the neuronal state. If this potential surpasses a threshold, the neuron fires a spike and the potential is reset; otherwise, it decays [2]. Thus, SNNs exhibit spike-based event-driven dynamics: sparse accumulations occur only upon spike transmissions between neurons, while the network stays idle otherwise [3]. Deploying SNNs on neuromorphic hardware [4, 5, 6] yields significant energy savings. For example, the asynchronous sensing-computing neuromorphic chip Speck consumes merely 0.42 mW at idle, and its dynamic power under typical vision scenarios can be kept within the mW range [7].

Directly training large-scale SNNs has long been a core challenge in the field. The progress can be viewed in three stages. i) Trainability under spike-based communication: surrogate-gradient methods [8, 9] were proposed to handle the non-differentiable spike activation function, so that SNNs can be trained with backpropagation algorithm. ii) Going deeper without performance loss: to reduce accuracy degradation in deeper SNNs, researchers introduced spiking residual connections [10, 11], novel architectures [12, 13, 14], various normalization methods [15], and training optimization methods [16, 17]. iii) Efficient training under complex spatiotemporal dynamic constraints: the goal is to study how to efficiently train larger SNNs under longer sequences, laying the foundation for directly training large spiking models.

Regarding the challenge mentioned in the third stage above, the reset mechanism prevents parallel training, which makes SNN training very costly. One line of work keeps reset but speeds up training by decoupling spatial and temporal dependencies, for example by dropping temporal dependence during backpropagation [18, 19], by letting only a subset of neurons carry temporal information [20, 21], or by using single-step pretraining followed by multi-step fine-tuning [22, 23]. Another line of work removes reset. PSN [1] first took this direction and added a learnable parameter matrix along the time dimension to compensate for the role of reset. Some subsequent studies

[24, 25] have improved upon PSN, but the resulting models lose the serial inference property inherent to vanilla spiking neurons, which enables efficient computation and stable extrapolation potential at test time. Another idea is to remove reset and approximate the membrane potential of vanilla spiking neuron [26, 27, 28]; this path is limited because the best possible performance cannot exceed that of the approximated neuron.

Given the popularity of large foundation models [29, 30], an in-depth understanding of spiking neuron parallelization is imperative for SNNs aiming to scale alongside them. To this end, this work takes a novel functional perspective to analyze what constitutes a good design for parallel training in SNNs. i) We begin by focusing on the reset of vanilla spiking neurons, identifying its functions as introducing nonlinearity and controlling the membrane potential, which enhances the temporal dynamics of spiking neurons and enables the modulation of the membrane potential. We also highlight the drawbacks of the reset mechanism, including its inability to adequately fulfill the data-dependent adaptive membrane potential update and its hindrance in parallel training. ii) We examine the general conditions under which spiking neurons support both parallel training and serial inference: their outputs depend solely on past inputs, allowing stepwise temporal iteration while supporting parallel computations across timesteps. These conditions serve as guiding principles for designing parallelized spiking neurons.

Based on these insights, we propose a dynamic decay spiking neuron with a causal convolution structure. Our approach can perform the functions of the reset mechanism more flexibly and thoroughly, while also supporting both parallel training and serial inference. We conduct comprehensive experiments to evaluate the proposed method, and the results demonstrate that our model outperforms existing parallel spiking neuron models in terms of training efficiency, extrapolation capability, generality, and energy efficiency. The key contributions of this work are as follows:

- **A Novel Functional View.** Parallel training in spiking neural networks is not merely about replacing the reset mechanism with a seemingly effective technique. Instead, it requires a systematic analysis of how the functions of reset are preserved or enhanced by the modification, and how parallel and serial modes can be made compatible under this change, which helps us understand the limitations of existing approaches.
- **Design under an Insightful Guideline.** Inspired by the functional perspective, we propose a dynamic decay spiking neuron that implements

functions better than reset, while supporting parallel training and remaining compatible with serial inference.

- **Generality.** Our method demonstrates consistently competitive performance across various network architectures and tasks, while also exhibiting training efficiency, stable extrapolation, and energy benefits.

2. Related Work

2.1. Spiking Neurons

The transmission of electrical signals in biological neurons can be modeled with differential equations. Common spiking neuron models include Hodgkin-Huxley neurons [31], Leaky Integrate-and-Fire (LIF) neurons [32], Izhikevich neurons [33], etc. Among these, LIF neurons are the preferred choice for training deep SNNs due to their simplicity [10]. Currently, the two main techniques for addressing the non-differentiability issue in deep SNNs are converting an artificial neural network (ANN) into its SNN counterpart [34, 35], i.e., ANN-to-SNN, and direct training methods [8, 9, 36, 23] which use surrogate gradients to implement backpropagation through time. In this paper, we focus on the latter approach. As spiking neural networks are being applied to more sequential processing tasks [37, 38, 39], how to strike a balance between constructing more complex spiking neurons and enabling efficient training has become an increasingly important concern.

2.2. Parallel Training in SNNs

Deep learning greatly benefits from large-scale parallel computing implemented on GPUs [40]. To realize parallel training in SNNs, existing methods mainly use parallelizable modules to directly replace the reset mechanism or approximate the membrane potential of vanilla spiking neurons. For the former, PSN [1] pioneers by introducing a learnable parameter matrix. In subsequent works, the alternatives focus primarily on the update method of membrane potential [41, 24, 25, 42] and the design of firing functions [43, 44, 45, 46]. However, most of them either abandon the inherent serial inference characteristics of vanilla spiking neurons or fail to fully preserve the functions of the reset mechanism. For the latter, the approximation methods for membrane potential range from a simple Bernoulli spike emission condition [26], a pre-trained surrogate dynamic network [27], to fixed-point iteration [28]. Moreover, Spike-SSM [47] deconstructs the membrane potential

and iteratively resolves the output spikes through parallel max-min boundary compression. Overall, without modifying the intrinsic neuron structure, these methods do not surpass vanilla spiking neurons in performance.

2.3. Decay Mechanism in Spiking Neuron

For SNNs, the decay factor, usually termed as the membrane time constant in LIF neurons, implies a limitation on expressiveness due to its fixed nature. PLIF [48] improves neuronal dynamics by making the decay factor learnable. Subsequent methods parameterize the decay factor via adjusting the parameter expression [1, 49, 50, 51, 52], integrating bidirectional parameters [25], introducing a complementary bypass [53]. In addition, some studies apply decay to the firing threshold [54, 55]. In dendritic neuron modeling, DH-LIF [56] learns multi-timescale dynamics by introducing heterogeneous decay factors across different dendritic branches. However, the decay factor remains static after training. In recent works, gating mechanisms [57, 58], adaptive membrane time constant [59] or self-connection circuit [60] have been employed to capture various biological features and enhance adaptiveness. What they have in common is that after training, the decay factor still changes with variations in input, membrane potential, and output spikes. This data-dependent paradigm inspires us to delve deeper into dynamic decay that is solely related to input.

3. A Functional View of Parallelizing Spiking Neurons

Removing the reset mechanism makes spiking neurons trainable in parallel. To understand what this change truly does, we need to answer two basic questions: **i) What is the function of reset; ii) Under what conditions can spiking neurons simultaneously support parallel training and serial inference.** The first question helps us identify the functional deficiencies of prior work in reconstructing spiking neurons, thereby motivating strategies to compensate for that function, or even improve upon it. The second question is fundamental to the efficient inference of SNNs.

3.1. Reset Mechanism and Its Function

Hard and Soft Reset. In biological neurons, the depolarized membrane potential is restored to the resting state after the soma fires a spike [61]. Spiking neurons abstract the neuronal dynamics described above. Considering the trade-off between bio-plausibility and computational efficiency, the most

widely used spiking neuron is the LIF, whose discrete iterative form is as follows [8]:

$$H_t = \beta V_{t-1} + (1 - \beta) X_t, \quad (1)$$

$$S_t = \Theta(H_t - V_{\text{th}}), \quad (2)$$

$$V_t = \begin{cases} H_t(1 - S_t) + V_{\text{reset}} S_t, & \text{hard reset} \\ H_t - V_{\text{th}} S_t, & \text{soft reset} \end{cases}. \quad (3)$$

In Eq. 1, the current input X_t is integrated with the membrane potential V_{t-1} from last timestep, and the decay factor $\beta = 1 - \frac{1}{\tau_m}$, where τ_m is membrane time constant. In Eq. 2, the Heaviside step function $\Theta(x) = 1$ when $x \geq 0$, i.e. the membrane potential H_t exceeds the threshold V_{th} , indicating that a spike is fired; otherwise, it is set to 0. According to how the membrane potential is regulated based on output spikes, reset can be generally categorized into hard and soft reset as depicted in Eq. 3. In hard reset, the charged membrane potential H_t will be set to a constant V_{reset} if a spike is fired, otherwise it will remain unchanged. V_{reset} is commonly set to 0 for simplicity. In contrast, soft reset subtracts H_t by V_{th} when a spike is fired.

Functions of Reset Mechanism. The first function is to **introduce nonlinearity**. Specifically, the reset mechanism enriches the temporal dynamics of spiking neurons by establishing the following nonlinear relationship between the membrane potential and the input:

Definition 3.1. If the expression $H_t = g(X_1, X_2, \dots, X_t)$ is not a linear equation, the hidden state with respect to the inputs is considered nonlinear.

Remark: Without reset, Eq. 1 can be expanded into a linear form with respect to input.

$$H_t = \sum_{i=1}^t \beta^{t-i} (1 - \beta) X_i. \quad (4)$$

In contrast, both hard and soft reset insert the firing function $f(\cdot)$ into the iteration of membrane potential at two adjacent timesteps. Taking hard reset

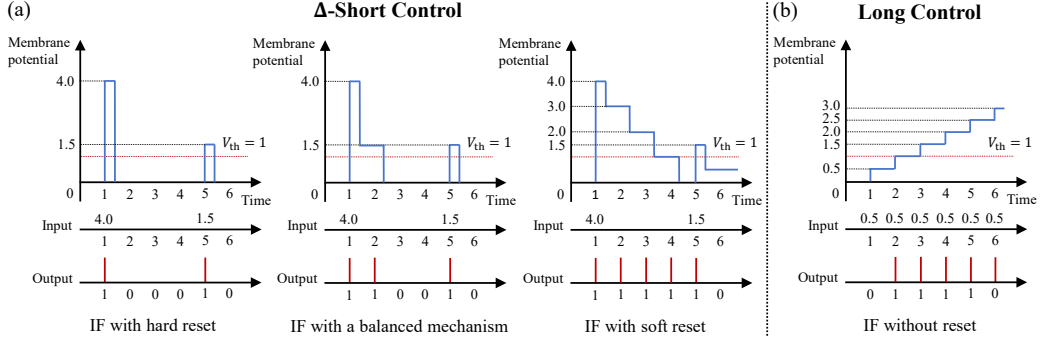


Figure 2: The reset mechanism serves the function of regulating the membrane potential in an input-dependent manner, which can be categorized into Δ -short and long control. (a) Δ -short control. *Left*: Hard reset enforces short control at $\Delta = 1$ level, but it does not allow spatial discriminability between inputs of varying importance. Regardless of how large the membrane potential is at the current timestep, it will be forcibly reset to zero if it exceeds the threshold. *Right*: Soft reset extends the control duration as the input magnitude increases, which can lead to continuous spike firing and reduced temporal discriminability. That is, compared to hard reset, soft reset allows the input at the current timestep to influence several subsequent timesteps; but it also introduces the challenge of making it difficult to distinguish which inputs across different timesteps are more important. *Middle*: We therefore seek a balanced mechanism that adaptively determines the duration of membrane potential influence based on the input. (b) Long control. Without reset, even under a relatively small constant input sequence, e.g., $\{0.5\}$, the membrane potential of a spiking neuron would continuously accumulate, leading to infinite spike firing.

as an example, if letting $V_{\text{reset}} = 0$ and combining Eq. 1 and Eq. 3, we will derive one-step iteration form of the membrane potential.

$$H_t = \beta(1 - f(H_{t-1}))H_{t-1} + (1 - \beta)X_t. \quad (5)$$

Obviously, it cannot be transformed into an input-dependent linear equation. This is similar for soft reset as well. Therefore, we conclude that reset introduces nonlinearity, and several parallel spiking neuron designs [1, 41, 46] ignore this role.

The second function is to **control membrane potential**. The reset mechanism constrains the membrane potential within a suitable range and averts ceaseless spike firing. For clarity, we quantitatively describe the control ability over the membrane potential as Δ -short control and long control:

Definition 3.2. There exists an $\Delta \in \mathbb{N}^+$ such that, for any $t > \Delta$, if

$H_{t-\Delta} \geq V_{\text{th}}$ and $X_{t-\Delta+1}, \dots, X_t < V_{\text{th}}/\Delta$, it always holds that $H_t < V_{\text{th}}$. In this case, the spiking neuron is said to have **Δ -short control** over the membrane potential.

Remark: The reset mechanism controls how long a large membrane potential affects the spiking neuron. For example, consider an IF neuron without a decay factor, with $V_{\text{th}} = 1$ and $H_1 = X_1 = 4$. In hard reset, the membrane potential is immediately set to 0 after a spike firing, so the effect of the large input lasts for $\Delta = 1$ timestep. In contrast, with a soft reset, the spike persists for 4 timesteps. Δ -short control ensures that a very large input affects the spiking neuron only within a relatively short time window Δ , thereby preventing prolonged spike firing (see Fig. 2).

Definition 3.3. If the input sequence $\{X_t\}$ has an upper bound C , then the membrane potential sequence $\{H_t\}$ also has an upper bound C_H . In this case, the spiking neuron is said to have **long control** over the membrane potential.

Remark: Long control prevents sustained spike firing or even membrane potential explosion caused by small inputs that accumulate without being reset (see Fig. 2). In other words, long control keeps the membrane potential stable over an arbitrarily long period of time.

Towards Better Functional Realization. Although we have identified two functions of reset, the reset mechanism itself is not the optimal realization of these functions. Specifically, the nonlinear response is binary—either 0 or 1—lacking diversity. More importantly, the control of membrane potential via hard or soft reset is highly rigid and lacks flexibility. In hard reset, regardless of how large the membrane potential becomes, its influence is terminated after a single timestep. This strict mechanism severely limits spatial discriminability, as spike generation cannot reflect differences in input magnitude beyond threshold. Conversely, soft reset subtracts a fixed amount from the membrane potential upon spiking. For large inputs, multiple timesteps are required to neutralize their accumulated effect, leading to prolonged spike firing. As a result, spike events become increasingly dependent on past inputs, degrading temporal discriminability and obscuring the contribution of the current input.

Therefore, in many existing parallel spiking neuron designs, structures that attempt to approximate either hard reset [27, 28] or soft reset [24, 43, 44] can at best reproduce functions similar to those of the reset mechanism, but cannot achieve functions beyond it. Recognizing the inherent limitations of reset helps us focus on enhancing the two functions abstracted from it.

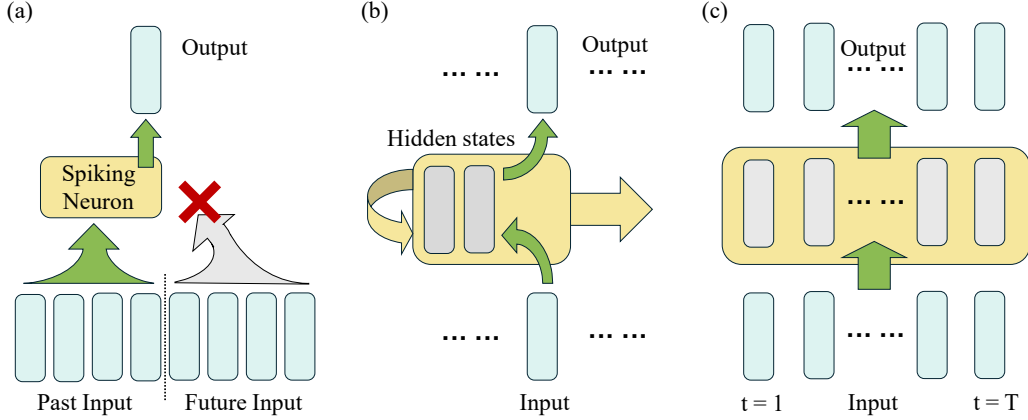


Figure 3: Illustration of the three conditions for spiking neurons to achieve parallel training and serial inference. (a) Condition 1: Prefix summarizability. The output can only be determined by inputs from the past (the prefix), and this dependency does not change over time. (b) Condition 2: Online updatability. The internal hidden states can be recurrently updated as the sequential input arrives. (c) Condition 3: Offline parallelizability. For a fixed-length sequence, the output can be computed via parallel computation through time.

3.2. Conditions for supporting parallel training and serial inference

A natural idea to realize parallel training in SNNs is to replace the reset mechanism with other parallelizable technique. However, some previous works [1, 24, 25] sacrifice the inherent efficiency of serial inference in vanilla spiking neurons, where the membrane potential at each timestep can be computed solely from the preceding membrane potential (or a small fixed set of states) and the current input. Consequently, such approaches introduce increased computational and memory overhead during inference and may even fail to generalize beyond the training sequence length.

We therefore argue that parallel training in SNNs should remain compatible with serial inference, allowing appropriate computational modes at different stages. Through observation and induction, we further identify three structural conditions that spiking neurons must satisfy to enable parallel training while retaining efficient serial inference.

Condition 1: Prefix Summarizability. At any time step t , the output S_t of the spiking neuron depends only on a representation H_t determined by the prefix $X_{1:t}$ (X_1, X_2, \dots, X_t).

$$\forall t \geq 1, H_t = \phi_\theta(X_{1:t}), S_t = g_{\theta'}(H_t) \quad (6)$$

Table 1: A review of vanilla spiking neurons and its typical parallel variants. Function 1: Introducing nonlinearity. Function 2: Controlling the membrane potential. PTSI: Parallel training and serial inference. Condition 1: Prefix summarizability. Condition 2: Online updatability. Condition 3: Offline parallelizability.

Methods	Functions of Reset		Conditions of PTSI		
	Function 1	Function 2	Condition 1	Condition 2	Condition 3
LIF [32]	✓	✓	✓	✓	✗
PSN [1]	✗	✗	✗	✗	✓
Masked PSN [1]	✗	✗	✗	✗	✓
Sliding PSN [1]	✗	✓	✓	✓	✓
PRF [43]	✗	✓	✓	✓	✓
IPSU [24]	✓	✗	✗	✗	✓
BPSN [25]	✗	✗	✗	✗	✓
DSN (Ours)	✓	✓	✓	✓	✓

Remark: This condition implicitly requires a specific structural relationship between the intermediate representation H and the input X . First, H_t must be causal, depending only on the prefix $X_{1:t}$ and not on any future inputs. Second, the prefix summary ϕ must be time-invariant, with parameters θ shared across all time steps.

Condition 2: Online Updatability. The prefix representation H_t can be updated online through a finite amount of computation during inference.

$$\forall t \geq 1, H_t = u_\theta(H_{t-1}, X_t) \quad (7)$$

Remark: This condition indicates that the membrane potential update process must reuse computation results from previous time steps.

Condition 3: Offline Parallelizability. All s_t within a window of size T can be obtained by parallel computation through time during training.

$$\exists p, \forall t \in [1, T], \text{ s.t. } H_t = p_\theta(X_{1:t}) \quad (8)$$

Remark: This condition suggests that, given the offline sequence $x_{1:T}$, there exists a computational graph (e.g., convolution, matrix multiplication, or parallel scan) for $H_{1:T}$ along the temporal dimension that is independent of the recursive execution order in Eq. 7.

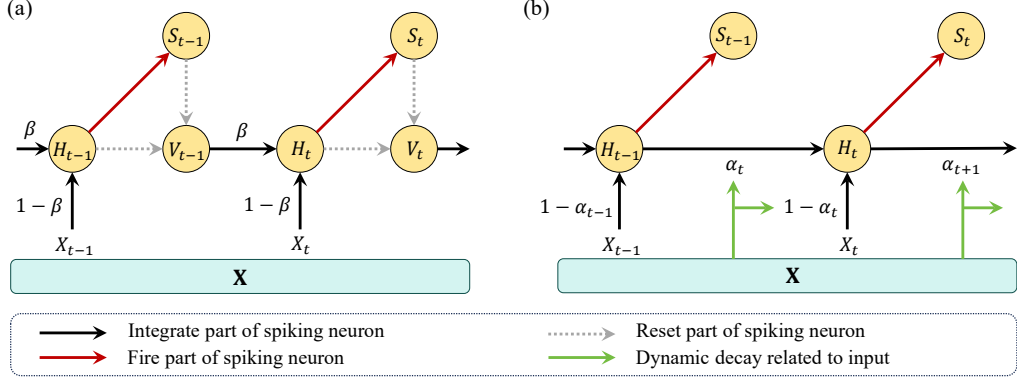


Figure 4: Illustration of the computational process of LIF spiking neuron and reset-free spiking neuron with dynamic decay. (a) LIF neuron. The current input and the membrane potential from last timestep are integrated with a constant decay factor β . The integrated H_t determines the firing of the spike S_t , which in turn decides whether H_t is reset. (b) Dynamic decay. After replacing the reset mechanism with dynamic decay α_t , the membrane potential can be computed both serially and in parallel.

As the conclusion of this section, Table 1 summarizes the extent to which various spiking neurons satisfy the functions of reset and the conditions required for enabling parallel training while remaining compatible with serial inference. It is worth noting that the early and well-known PSN and Masked PSN [1] have learnable parameters coupled with the training timestep, and thus fail to satisfy Conditions 1 and 2. More critically, PSN cannot guarantee causality in sequential computations, and its number of parameters grows quadratically with the sequence length, thereby incurring substantial computational overhead. Therefore, they are not ideal candidates for parallelizable spiking neurons. Instead, the parallelizable spiking neuron we seek should not only preserve—or even enhance—the two functions of reset, but also satisfy the three conditions required for parallel training and serial inference.

4. Methods: Dynamic Decay Spiking Neuron

Sec. 3 provides general guidance for designing parallelizable spiking neurons through the lens of functional analysis. Building on this, we propose a Dynamic Decay Spiking Neuron (**DSN**), which includes two modifications to vanilla spiking neurons: i) the reset mechanism is removed and the constant decay β is replaced with a dynamic decay α_t . Here, α_t is obtained via a

causal convolution over the input. ii) the spike firing pattern is optimized by incorporating emerging integer-valued training techniques [62]. DSN has the following vectorized serial form:

$$\mathbf{H}_t = \boldsymbol{\alpha}_t \odot \mathbf{H}_{t-1} + (1 - \boldsymbol{\alpha}_t) \odot \mathbf{X}_t. \quad (9)$$

$$\mathbf{S}_t = \text{Clip}[\text{Round}(\mathbf{H}_t), 0, N]. \quad (10)$$

Here, the input $\mathbf{X}_t \in \mathbb{R}^{C \times 1}$ has C channels. \odot denotes element-wise product. $\text{Round}(\cdot)$ indicates rounding to the nearest integer. $\text{Clip}[x, 0, N]$ means clipping the input x to the range $[0, N]$. N is a positive integer, representing the upper limit of the number of spikes to be emitted.

In Eq. 9, we derive the dynamic decay $\boldsymbol{\alpha}_t$ from $\mathbf{X}_{t-k+1:t}$ (k inputs from \mathbf{X}_{t-k+1} to \mathbf{X}_t) as follows:

$$\boldsymbol{\alpha}'_t = \text{CausalConv1D}(\mathbf{X}_{t-k+1:t}), \quad (11)$$

$$\boldsymbol{\alpha}_t = \text{Sigmoid}(\boldsymbol{\alpha}'_t)^{1/\tau} \quad (12)$$

Here, $\text{CausalConv1D}(\cdot)$ is a causal 1D convolution to mix the features from the past k inputs. Sigmoid function is chosen to constrain $\boldsymbol{\alpha}_t$ between 0 and 1. τ is a hyperparameter to fine-tune $\boldsymbol{\alpha}_t$.

Design Rationale. After removing the reset mechanism, we find that a varying decay factor can also introduce nonlinearity and control membrane potential, thereby restoring the functions of reset. This forms the basis of our initial design. The causal convolution is usually short but has been shown to be effective in capturing short-term dependency [63, 64]. The optimized spike firing pattern helps reduce training overhead and learn better representations [65]. Moreover, we can choose to introduce an extra learnable parameter $\mathbf{W} \in \mathbb{R}^{C \times C}$ to mix the features across different channels of $\boldsymbol{\alpha}'_t$ before applying the Sigmoid function in Eq. 12, i.e. $\mathbf{W}\boldsymbol{\alpha}'_t$. This enhanced DSN is suitable as a complete block to further improve the modeling ability of SNNs.

Functions Superior to Reset. DSN is a specific implementation of dynamic decay α_t , which can be related to input at preceding timesteps and is usually limited to between 0 and 1 using a non-linear activation function with learnable parameters θ :

$$\alpha_t = \phi_\theta(X_t, X_{t-1}, \dots) \in [0, 1] \quad (13)$$

In fact, we can prove that dynamic decay in Eq. 13 can implement all the

functions of reset.

Proposition 4.1. *Dynamic decay can introduce nonlinearity and enabling more flexible Δ -short and long control of the membrane potential than the reset mechanism.*

Remark: We provide the detailed proof in Appendix A.2. An intuitive interpretation is that the variability of α_t broadens the expressive range of nonlinearity and allows adaptive control of the membrane potential. Additionally, the proposition holds for both binary and integer-valued spike firing, showing that dynamic decay is a general and powerful alternative to reset.

From Serial Inference to Parallel Training. After removing the reset mechanism, DSN retains the iterative nature of vanilla spiking neurons while supporting a parallelizable computation graph. This satisfies the three conditions described in Sec. 3.2, enabling parallel training. Specifically, Eq. 9 can be rewritten into a general form determined solely by $\mathbf{X}_1, \mathbf{X}_2, \dots, \mathbf{X}_t$:

$$\mathbf{H}_t = \sum_{i=1}^t \left(\prod_{j=i+1}^t \boldsymbol{\alpha}_j \right) (\mathbf{1} - \boldsymbol{\alpha}_i) \odot \mathbf{X}_i. \quad (14)$$

Stacking $\mathbf{H}_1, \mathbf{H}_2, \dots, \mathbf{H}_T$ gives $\mathbf{H} \in \mathbb{R}^{C \times T}$, and similarly for $\mathbf{X} \in \mathbb{R}^{C \times T}$. This allows expressing the iterative computation in a matrix form $\mathbf{H} = \mathbf{X}\mathbf{W}$, where

$$\mathbf{W}_{ij} = \begin{cases} \left(\prod_{k=i+1}^j \boldsymbol{\alpha}_k \right) (\mathbf{1} - \boldsymbol{\alpha}_i), & j \geq i \\ 0, & j < i \end{cases}. \quad (15)$$

Define $\mathbf{P}, \mathbf{A} \in \mathbb{R}^{C \times T}$, $\mathbf{M} \in \mathbb{R}^{T \times T}$, where

$$\mathbf{P}_j = \prod_{k=1}^j \boldsymbol{\alpha}_k, \mathbf{A}_i = \boldsymbol{\alpha}_i, \mathbf{M}_{ij} = \begin{cases} 1, & j \geq i \\ 0, & j < i \end{cases}. \quad (16)$$

Then, the parallel form can be written as:

$$\mathbf{H} = \mathbf{X} \left(\left(\left(\frac{\mathbf{1} - \mathbf{A}}{\mathbf{P}} \right)^T \mathbf{P} \right) \odot \mathbf{M} \right) \quad (17)$$

Here, $\frac{\mathbf{1} - \mathbf{A}}{\mathbf{P}}$ and \odot denote element-wise division and product, respectively. During training, the dynamic decay \mathbf{A} , membrane potential \mathbf{H} and their

gradients can be computed rapidly in parallel¹ with Triton-based acceleration operators [68, 69]. During inference, we switch to Eq. 9 for efficient serial inference, which requires to store only minimal states from the causal convolution and recurrent structure, thereby reducing both computational and memory overhead.

5. Experiments

In this section, we evaluate the proposed DSN through a series of experiments in terms of

- **Training Efficiency and Extrapolation.** We demonstrate that DSN achieves significant speedups over existing parallelizable spiking neurons on long sequences, and show through a text extrapolation experiment that serial inference is an inherent and indispensable property of spiking neurons.
- **Generality.** The neuronal generality includes: i) The effectiveness of spiking neuron design, including the causal convolution structure and two spike activation modes (binary and integer); ii) Flexible adaptation to various network architectures, such as convolutional neural networks and Transformers; iii) Competitive performance across five different tasks.
- **Energy Consumption.** We discuss the potential of DSN for deployment on neuromorphic hardware and conduct a preliminary analysis of its energy efficiency compared with prior parallel spiking neurons.

5.1. Training Efficiency and Extrapolation

Parallel Training Improves Efficiency. We evaluate the training efficiency of different parallelizable spiking neurons by measuring the average runtime of 100 forward and backward passes under varying sequence lengths. From the results in Fig. 5 left, it can be observed that the speedup of DSN over PSN [1] becomes increasingly pronounced as the sequence length grows. For sequences of length 16k, DSN achieves a $21.7\times$ speedup in the forward pass and a $28.0\times$ speedup in the backward pass compared to PSN, resulting in an overall runtime speedup of $25.6\times$. For Sliding PSN [1], a parameter-efficient

¹In practice, we avoid computing \mathbf{H} via matrix multiplication due to numerical instability of \mathbf{P} as the denominator [66]. Instead, we use a two-stage parallel scan algorithm [67] for Eq. 9 to derive \mathbf{H} .

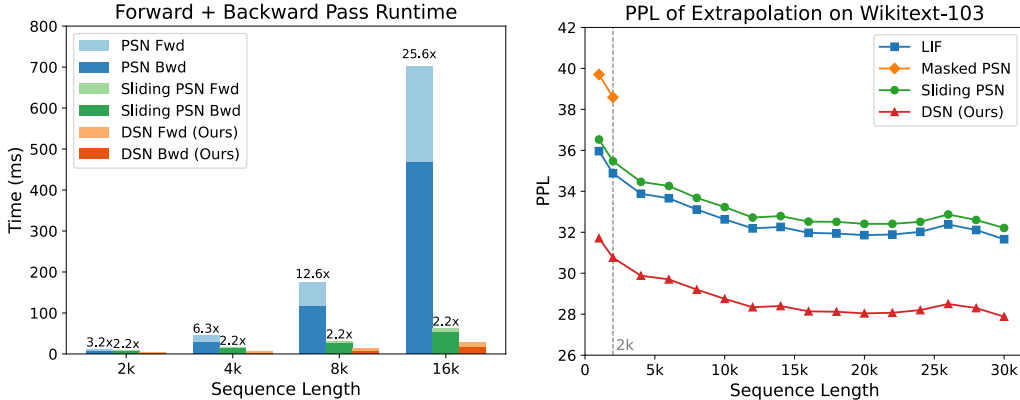


Figure 5: Results of training efficiency (left) and extrapolation (right). Left: Runtime of the forward and backward pass when training on sequences with lengths from 1k to 8k. Right: Perplexity (PPL, the lower the better) of extrapolation on WikiText-103 with sequence lengths ranging from 1k to 30k, trained on sequences of length 2k.

variant of PSN, on sequences of length 16k, although DSN is slightly slower in the forward pass, its $3.2\times$ faster backward pass leads to an overall training speed that is still $2.2\times$ faster than Sliding PSN.

Serial Inference Ensures Extrapolation. In sequence tasks such as language modeling, models are often required to extrapolate to sequences longer than those seen during training. While vanilla spiking neurons can operate on sequences of arbitrary length, some parallelized spiking neurons lose serial inference ability and are therefore limited in extrapolation. To evaluate the extrapolation ability of DSN, we conduct experiments on WikiText-103 [70] dataset using SpikingSSM [27] architecture with different spiking neurons. Models are trained on sequences of length 2k and evaluated on longer sequences by measuring perplexity. As shown in Fig. 5 right, masked PSN [1] fails beyond 2k tokens, whereas DSN maintains stable performance on sequences up to 30k tokens and outperforms LIF and sliding PSN [1].

5.2. Generality

5.2.1. Effectiveness of Spiking Neuron Design

We evaluate the effectiveness of spiking neuron design on Sequential CIFAR10, including the causal convolution structure and different spike activation modes. Results in Table 2 and 3 show that:

First, dynamic decay is the primary contributor to performance. Removing the causal convolution eliminates meaningful neuronal dynamics and leads to a significant degradation (84.53%). We also test alternative decay structures, including fully connected layers for inter-channel interaction, low-rank mappings, and inter-channel convolution. In comparison, causal convolution remains a simple yet effective design.

Second, dynamic decay is effective for both binary ($N = 1$) and integer-valued ($N > 1$) spike firing. In the binary mode, using Arc Tangent as the surrogate gradient function yields better performance. In the integer-valued mode, the performance improves with increasing spike limit N .

Based on the above experiments, we design DSN by combining causal convolution with an integer-valued training technique, and validate its generality across different model architectures and tasks.

5.2.2. Generality Across Multiple Tasks

We evaluate DSN across five tasks: image classification, neuromorphic event processing, time-series forecasting, reinforcement learning, and language modeling, using models that span convolutional neural networks, Transformers, and State Space Models (SSMs). Competitive results across multiple datasets and network architectures demonstrate the general effectiveness of DSN.

Sequential CIFAR. we build a convolution-based SNN on Sequential CIFAR dataset, where the images from CIFAR [74] are input into the model in sequential pixel form and the timestep is equal to the width 32 of the images. The experimental setup and other hyperparameters are kept consistent with those of PSN [1]. Results in Table 4 show that our DSN achieves state-of-the-art performance under the same parameter scale.

ImageNet. We further evaluate the performance of DSN on this larger-scale image classification task [75]. The experimental settings are identical

Table 2: Ablations: different design of dynamic decay structure.

Methods	Accuracy (%)
causal conv	90.10
fully connected layer	89.28
low-rank mapping	86.72
inter-channel conv	86.76
w/o conv	84.53

Table 3: Ablations: spike activation modes. N : the maximum spike count. Rect: Rectangular. ATan: Arc Tangent.

N	Surrogate Grad	Accuracy (%)
4	Rect	90.10
3	Rect	89.56
2	Rect	89.28
1	Rect	86.74
1	ATan	87.45

Table 4: Performance on Sequential CIFAR. The timestep is 32. Param: parameters (M).

Methods	Parallel	Serial	S-CIFAR10		S-CIFAR100	
			Param.	Accuracy (%)	Param.	Accuracy (%)
LIF [32]	\times	\checkmark	0.513	81.50	0.537	55.45
PLIF [48]	\times	\checkmark	0.513	81.50	0.537	55.45
PSN [1]	\checkmark	\times	0.521	88.45	0.544	62.21
RPSU [24]	\checkmark	\times	0.517	84.44	0.540	57.89
IPSU [24]	\checkmark	\times	0.517	87.28	0.540	59.76
Sliding PSN [1]	\checkmark	\checkmark	0.514	86.70	0.538	62.11
DSN (Ours)	\checkmark	\checkmark	0.519	90.10	0.542	64.70

Table 5: Performance on ImageNet and CIFAR10-DVS. T: Timesteps.

Dataset	Methods	Architecture	Parallel	Serial	T	Accuracy (%)
ImageNet	MBPN [71]	ResNet18	\times	\checkmark	4	63.14
	InfLoR-SNN [72]	ResNet18	\times	\checkmark	4	64.78
	SEW ResNet [10]	SEW ResNet18	\times	\checkmark	4	63.18
	PMSN [44]	SEW ResNet18	\checkmark	\checkmark	4	66.64
	PSN [1]	SEW ResNet18	\checkmark	\times	4	67.63
DSN (Ours)		SEW ResNet18	\checkmark	\checkmark	4	68.21
CIFAR10-DVS	SEW ResNet [10]	Wide 7B Net	\times	\checkmark	16	74.40
	GLIF [57]	Wide 7B Net	\times	\checkmark	16	78.10
	DeepTAGE [73]	VGG-11	\times	\checkmark	10	81.23
	RPSU [24]	VGGSNN	\checkmark	\times	10	82.00
	FPT [28]	VGG-11	\checkmark	\times	10	85.50
sliding PSN [1]		VGGSNN	\checkmark	\checkmark	4, 8	82.30, 85.30
DSN (Ours)		VGGSNN	\checkmark	\checkmark	4, 8	83.90, 85.30

to [1]. For a fair comparison, we follow [65] and set the training step T of DSN to 1, while treating the upper bound $N = 4$ of integer-spike emission as the extended timestep T . As illustrated in Table 5, our method still achieves relatively higher accuracy among parallel spiking neurons.

CIFAR10-DVS. To validate the effectiveness of our method in processing neuromorphic events, we select CIFAR10-DVS [76] as the benchmark and

Table 6: Experimental results of 3 time-series forecasting tasks with prediction lengths $L = 6, 24, 48, 96$. \uparrow (\downarrow) indicates the higher (lower) the better. All results are averaged across 3 random seeds. The leading zero before the decimal point is omitted. Param: parameters (M).

Methods	Spike	Param.	Metric	Metr-la				Pems-bay				Solar				Avg.
				6	24	48	96	6	24	48	96	6	24	48	96	
Transformer	\times	2.53	$R^2\uparrow$.727	.554	.413	.284	.785	.734	.688	.673	.953	.858	.759	.718	.679
			RSE \downarrow	.551	.704	.808	.895	.502	.558	.610	.618	.223	.377	.504	.545	.575
Spikformer	\checkmark	2.52	$R^2\uparrow$.713	.527	.399	.267	.773	.697	.686	.667	.929	.828	.744	.674	.659
			RSE \downarrow	.565	.725	.818	.903	.514	.594	.606	.621	.272	.426	.519	.586	.596
Spikformer w/ PSN	\checkmark	2.68	$R^2\uparrow$.716	.518	.401	.268	.738	.671	.666	.639	.861	.759	.554	.439	.603
			RSE \downarrow	.562	.731	.815	.901	.553	.620	.624	.649	.383	.504	.685	.749	.648
Spikformer w/ DSN	\checkmark	2.68	$R^2\uparrow$.734	.549	.422	.283	.807	.745	.696	.683	.956	.860	.765	.736	.686
			RSE \downarrow	.539	.720	.804	.896	.475	.538	.581	.594	.219	.373	.481	.572	.566
iTransformer	\times	1.63	$R^2\uparrow$.829	.623	.439	.285	.887	.719	.685	.668	.964	.879	.799	.738	.710
			RSE \downarrow	.436	.648	.780	.878	.362	.547	.561	.584	.191	.348	.448	.563	.529
iSpikformer	\checkmark	1.63	$R^2\uparrow$.817	.618	.440	.279	.879	.744	.687	.674	.961	.876	.795	.738	.709
			RSE \downarrow	.475	.668	.752	.905	.376	.536	.569	.580	.204	.333	.465	.521	.532
iSpikformer w/ DSN	\checkmark	1.79	$R^2\uparrow$.823	.624	.440	.283	.883	.740	.689	.672	.964	.879	.798	.736	.711
			RSE \downarrow	.450	.646	.755	.881	.368	.541	.564	.583	.199	.350	.450	.526	.526

adopt the VGG architecture from [77]. As shown in Table 5, DSN shows performance comparable to sliding PSN and ranks just below FPT [28], which employs a PSN-like structure and therefore cannot perform serial inference.

Time-series Forecasting Tasks. On more realistic time-series forecasting tasks, we adapt DSN to the following datasets: Metr-la [78]: traffic flow records from Los Angeles; Pems-bay [78]: traffic flow records from the San Francisco Bay Area; Solar [79]: solar power generation data. Baseline architectures include Transformer [80], iTransformer [81], and their respective SNN counterparts [12, 39]. For all SNN-based time-series forecasting models, we replace the original LIF neurons with DSN and make architectural modifications (see Appendix B.3). The Root Relative Squared Error (RSE) and the coefficient of determination (R^2) are used as metrics. It can be seen from Table 6 that DSN-based architectures exhibit superior performance on various tasks and prediction lengths.

Reinforcement Learning. Following Xu et al. [86], we evaluate DSN on three off-policy reinforcement learning benchmarks: IDP-v4 [87], Hopper-v4 [88], and Walker2d-v4. Table 7 reports the average returns of DSN across these environments, in comparison with several representative baselines, in-

Table 7: Reinforcement learning results on three representative benchmarks.

Methods	IDP-v4	Hopper-v4	Walker2d-v4
ANN (TD3)	7503 ± 3713	3410 ± 164	4340 ± 383
ANN-SNN [82]	3859 ± 4440	3098 ± 281	4235 ± 354
Vanilla LIF	9347 ± 1	3520 ± 94	1862 ± 1450
pop-SAN [83]	9351 ± 1	2772 ± 1263	3307 ± 1514
MDC-SAN [84]	9350 ± 1	3446 ± 131	3964 ± 1353
ILC-SAN [85]	9352 ± 1	3403 ± 148	4200 ± 717
PT-LIF [86]	9348 ± 1	3385 ± 157	4314 ± 423
DSN (Ours)	9354 ± 1	3565 ± 68	4436 ± 196

cluding ANN-based RL methods, ANN-to-SNN conversion approaches [82], and state-of-the-art SNN-based RL algorithms such as pop-SAN [83], MDC-SAN [84], ILC-SAN [85], and PT-LIF [86]. Detailed experimental configurations are provided in Appendix B.4. Overall, DSN achieves state-of-the-art performance on all three benchmarks. Moreover, compared with existing SNN-based methods, DSN consistently attains both superior average returns and reduced variance, indicating improved stability during training.

WikiText-103. To demonstrate that DSN can model more complex sequences such as language, we evaluate its perplexity on WikiText-103 [70], a large-scale word-level dataset constructed from the English Wikipedia. Following SpikingSSM [27], we use the S4D architecture [90] and replace its spiking neurons with DSN. Results in Table 8 show that DSN performs the best among spiking language models.

5.3. Energy Consumption

Neuromorphic Chip Deployment. There are still some gaps before DSN can be deployed on neuromorphic chips. On the one hand, dynamic decay introduces more complex floating-point operations, such as convolutions and Sigmoid functions. To alleviate the hardware adaptation burden, further algorithmic optimizations are possible. For example, instead of performing

Table 8: Experimental results on WikiText-103 dataset. \downarrow indicates the lower the better. \dagger means the results reported by [47]. Param: parameters (M). PPL: perplexity.

Methods	Param.	PPL \downarrow
SpikeGPT † [89]	213	39.75
SPikE-SSM † [47]	75.4	33.18
SpikingSSM [27]	75.4	32.25
DSN (Ours)	75.5	28.50

Table 9: Spike firing rate (SFR.) and energy cost (mJ) of different methods.

Methods	S-CIFAR10		S-CIFAR100	
	SFR.	Energy Cost	SFR.	Energy Cost
LIF [32]	0.1499	107.80	0.1697	121.78
PSN [1]	0.2143	235.87	0.2226	242.03
Sliding PSN [1]	0.1820	170.39	0.1900	176.22
DSN (Ours)	0.1238	102.89	0.1324	108.94

multiplications between floating-point weights and activations, the weights can be quantized to ternary values ($-1, 0, 1$) [91, 92], or a spiking function can be inserted to convert floating-point inputs into spikes in advance. For the Sigmoid function, the exponential base can be replaced with 2 to enable lightweight computations using shift operations [93]. On the other hand, prior work shows that integer outputs can be converted into asynchronously emitted spikes on neuromorphic hardware [65], providing a clear direction for hardware-oriented adaptation of optimized spike firing patterns.

Energy Consumption. Compared to vanilla spiking neurons, DSN affects energy consumption in two main aspects. i) The adaptive regulation of membrane potential help reduce the spike firing rate, thereby lowering the overall energy cost. ii) The complex floating-point operations in dynamic decay structures inevitably incur additional energy overhead. To evaluate the potential of DSN in terms of energy efficiency, we estimate the energy cost of the Sequential CIFAR network with different spiking neurons by following the method in [13]. For internal neuron operations, we refer to [93] where exponential operations in functions such as Softmax or Sigmoid can be transformed into additions and bit-shift operations. Results in Table 9 show that although additional modules such as convolution operations were introduced, the total energy consumption of DSN can be slightly lower than that of LIF due to its reduced spike firing rate. Additionally, PSN exhibits the highest spike firing rate, which in turn results in relatively high energy consumption. See Appendix B.6 for more details.

6. Conclusion

In this paper, we identify a critical limitation in existing efforts toward parallel training in SNNs: the neglect of preserving essential characteristics of vanilla spiking neurons, including the functions of the reset mechanism and the capability for serial inference. Under a new functional viewpoint, we summarize the functions of the reset mechanism in vanilla spiking neurons as introducing nonlinearity and controlling membrane potential. Meanwhile, we identify three conditions that spiking neurons need to meet in order to enable both parallel training and serial inference. Based on this general perspective, we introduce a dynamic decay spiking neuron that offers improved functions compared to reset while remaining compatible with serial inference. We verify the competitive training efficiency, stable extrapolation, generality across multiple tasks, and energy consumption of our method. Our work offers new insights into the exploration of high-performance spiking neurons with efficient training and inference abilities in the era of foundation models.

Reproducibility Statement

The authors have made great efforts to ensure the reproducibility of the empirical results reported in this paper. The experiment settings, evaluation metrics, and datasets were described in detail in Appendix B. Additionally, we had submitted the source code of the proposed training algorithm with our paper, and plan to release the source code on GitHub upon acceptance.

Acknowledgments

The authors would like to thank the anonymous reviewers for their valuable comments.

References

- [1] Wei Fang, Zhaofei Yu, Zhaokun Zhou, Ding Chen, Yanqi Chen, Zhengyu Ma, Timothée Masquelier, and Yonghong Tian. Parallel spiking neurons with high efficiency and ability to learn long-term dependencies. In Alice Oh, Tristan Naumann, Amir Globerson, Kate Saenko, Moritz Hardt, and Sergey Levine, editors, *Advances in Neural Information Processing Systems 36: Annual Conference on Neural Information Processing Systems*

2023, *NeurIPS 2023, New Orleans, LA, USA, December 10 - 16, 2023*, 2023.

- [2] Wolfgang Maass. Networks of spiking neurons: the third generation of neural network models. *Neural Networks*, 10(9):1659–1671, 1997.
- [3] Kaushik Roy, Akhilesh Jaiswal, and Priyadarshini Panda. Towards spike-based machine intelligence with neuromorphic computing. *Nature*, 575(7784):607–617, 2019.
- [4] Paul A Merolla, John V Arthur, Rodrigo Alvarez-Icaza, Andrew S Cassidy, Jun Sawada, Filipp Akopyan, Bryan L Jackson, Nabil Imam, Chen Guo, Yutaka Nakamura, et al. A million spiking-neuron integrated circuit with a scalable communication network and interface. *Science*, 345(6197):668–673, 2014.
- [5] Mike Davies, Narayan Srinivasa, Tsung-Han Lin, Gautham Chinya, Yongqiang Cao, Sri Harsha Choday, Georgios Dimou, Prasad Joshi, Nabil Imam, Shweta Jain, et al. Loihi: A neuromorphic manycore processor with on-chip learning. *IEEE Micro*, 38(1):82–99, 2018.
- [6] Jing Pei, Lei Deng, Sen Song, Mingguo Zhao, Youhui Zhang, Shuang Wu, Guanrui Wang, Zhe Zou, Zhenzhi Wu, Wei He, et al. Towards artificial general intelligence with hybrid tianjic chip architecture. *Nature*, 572(7767):106–111, 2019.
- [7] Man Yao, Ole Richter, Guangshe Zhao, Ning Qiao, Yannan Xing, Dingheng Wang, Tianxiang Hu, Wei Fang, Tugba Demirci, Michele De Marchi, et al. Spike-based dynamic computing with asynchronous sensing-computing neuromorphic chip. *Nature Communications*, 15(1):4464, 2024.
- [8] Yujie Wu, Lei Deng, Guoqi Li, Jun Zhu, and Luping Shi. Spatio-temporal backpropagation for training high-performance spiking neural networks. *Frontiers in Neuroscience*, 12:331, 2018.
- [9] Emre O Neftci, Hesham Mostafa, and Friedemann Zenke. Surrogate gradient learning in spiking neural networks: Bringing the power of gradient-based optimization to spiking neural networks. *IEEE Signal Processing Magazine*, 36(6):51–63, 2019.

- [10] Wei Fang, Zhaofei Yu, Yanqi Chen, Tiejun Huang, Timothée Masquelier, and Yonghong Tian. Deep residual learning in spiking neural networks. In Marc’Aurelio Ranzato, Alina Beygelzimer, Yann N. Dauphin, Percy Liang, and Jennifer Wortman Vaughan, editors, *Advances in Neural Information Processing Systems 34: Annual Conference on Neural Information Processing Systems 2021, NeurIPS 2021, December 6-14, 2021, virtual*, pages 21056–21069, 2021.
- [11] Yifan Hu, Lei Deng, Yujie Wu, Man Yao, and Guoqi Li. Advancing spiking neural networks toward deep residual learning. *IEEE Transactions on Neural Networks and Learning Systems*, 36(2):2353–2367, 2025. doi: 10.1109/TNNLS.2024.3355393.
- [12] Zhaokun Zhou, Yuesheng Zhu, Chao He, Yaowei Wang, Shuicheng Yan, Yonghong Tian, and Li Yuan. Spikformer: When spiking neural network meets transformer. In *The Eleventh International Conference on Learning Representations, ICLR 2023, Kigali, Rwanda, May 1-5, 2023*. OpenReview.net, 2023.
- [13] Man Yao, Jiakui Hu, Zhaokun Zhou, Li Yuan, Yonghong Tian, Bo Xu, and Guoqi Li. Spike-driven transformer. In Alice Oh, Tristan Naumann, Amir Globerson, Kate Saenko, Moritz Hardt, and Sergey Levine, editors, *Advances in Neural Information Processing Systems 36: Annual Conference on Neural Information Processing Systems 2023, NeurIPS 2023, New Orleans, LA, USA, December 10 - 16, 2023*, 2023.
- [14] Man Yao, JiaKui Hu, Tianxiang Hu, Yifan Xu, Zhaokun Zhou, Yonghong Tian, Bo XU, and Guoqi Li. Spike-driven transformer v2: Meta spiking neural network architecture inspiring the design of next-generation neuromorphic chips. In *The Twelfth International Conference on Learning Representations*, 2024.
- [15] Hanle Zheng, Yujie Wu, Lei Deng, Yifan Hu, and Guoqi Li. Going deeper with directly-trained larger spiking neural networks. In *Proceedings of the AAAI Conference on Artificial Intelligence*, volume 35, pages 11062–11070, 2021.
- [16] Yuhang Li, Yufei Guo, Shanghang Zhang, Shikuang Deng, Yongqing Hai, and Shi Gu. Differentiable spike: Rethinking gradient-descent for

training spiking neural networks. In *Advances in Neural Information Processing Systems*, volume 34, pages 23426–23439, 2021.

[17] Yufei Guo, Yuanpei Chen, Liwen Zhang, Xiaode Liu, Yinglei Wang, Xuhui Huang, and Zhe Ma. Im-loss: Information maximization loss for spiking neural networks. In *Advances in Neural Information Processing Systems*, volume 35, pages 156–166, 2022.

[18] Mingqing Xiao, Qingyan Meng, Zongpeng Zhang, Di He, and Zhouchen Lin. Online training through time for spiking neural networks. In Sanmi Koyejo, S. Mohamed, A. Agarwal, Danielle Belgrave, K. Cho, and A. Oh, editors, *Advances in Neural Information Processing Systems 35: Annual Conference on Neural Information Processing Systems 2022, NeurIPS 2022, New Orleans, LA, USA, November 28 - December 9, 2022*, 2022.

[19] Qingyan Meng, Mingqing Xiao, Shen Yan, Yisen Wang, Zhouchen Lin, and Zhi-Quan Luo. Towards memory- and time-efficient backpropagation for training spiking neural networks. In *IEEE/CVF International Conference on Computer Vision, ICCV 2023, Paris, France, October 1-6, 2023*, pages 6143–6153. IEEE, 2023. doi: 10.1109/ICCV51070.2023.00567.

[20] Jiakui Hu, Man Yao, Xuerui Qiu, Yuhong Chou, Yuxuan Cai, Ning Qiao, Yonghong Tian, Bo Xu, and Guoqi Li. High-performance temporal reversible spiking neural networks with $O(L)$ training memory and $O(1)$ inference cost. In *Forty-first International Conference on Machine Learning, ICML 2024, Vienna, Austria, July 21-27, 2024*. OpenReview.net, 2024.

[21] Changqing Xu, Guoqing Sun, Yi Liu, Xinfang Liao, and Yintang Yang. Pararevsnn: A parallel reversible spiking neural network for efficient training and inference. *CoRR*, abs/2508.01223, 2025. doi: 10.48550/ARXIV.2508.01223.

[22] Yihan Lin, Yifan Hu, Shijie Ma, Dongjie Yu, and Guoqi Li. Rethinking pretraining as a bridge from anns to snns. *IEEE Trans. Neural Networks Learn. Syst.*, 35(7):9054–9067, 2024. doi: 10.1109/TNNLS.2022.3217796.

[23] Man Yao, Guangshe Zhao, Hengyu Zhang, Yifan Hu, Lei Deng, Yonghong Tian, Bo Xu, and Guoqi Li. Attention spiking neural networks. *IEEE*

Transactions on Pattern Analysis and Machine Intelligence, 45(8):9393–9410, 2023.

- [24] Yang Li, Yinqian Sun, Xiang He, Yiting Dong, Dongcheng Zhao, and Yi Zeng. Parallel spiking unit for efficient training of spiking neural networks. In *2024 International Joint Conference on Neural Networks (IJCNN)*, pages 1–8. IEEE, 2024.
- [25] Qiaoyi Su, Shijie Mei, Xingrun Xing, Man Yao, Jiajun Zhang, Bo Xu, and Guoqi Li. Snn-bert: Training-efficient spiking neural networks for energy-efficient bert. *Neural Networks*, 180:106630, 2024.
- [26] Hanqi Chen, Lixing Yu, Shaojie Zhan, Penghui Yao, and Jiankun Shao. Time-independent spiking neuron via membrane potential estimation for efficient spiking neural networks. In *ICASSP 2025 - 2025 IEEE International Conference on Acoustics, Speech and Signal Processing (ICASSP)*, pages 1–5, 2025. doi: 10.1109/ICASSP49660.2025.10890472.
- [27] Shuaijie Shen, Chao Wang, Renzhuo Huang, Yan Zhong, Qinghai Guo, Zhichao Lu, Jianguo Zhang, and Luziwei Leng. Spikingssms: Learning long sequences with sparse and parallel spiking state space models. In Toby Walsh, Julie Shah, and Zico Kolter, editors, *AAAI-25, Sponsored by the Association for the Advancement of Artificial Intelligence, February 25 - March 4, 2025, Philadelphia, PA, USA*, pages 20380–20388. AAAI Press, 2025. doi: 10.1609/AAAI.V39I19.34245.
- [28] Wanjin Feng, Xingyu Gao, Wenqian Du, Hailong Shi, Peilin Zhao, Pengcheng Wu, and Chunyan Miao. Efficient parallel training methods for spiking neural networks with constant time complexity. In *Forty-second International Conference on Machine Learning, ICML 2025, Vancouver, Canada, July 13-19, 2025*, 2025.
- [29] Rishi Bommasani, Drew A Hudson, Ehsan Adeli, Russ Altman, Simran Arora, Sydney von Arx, Michael S Bernstein, Jeannette Bohg, Antoine Bosselut, Emma Brunskill, et al. On the opportunities and risks of foundation models. *arXiv preprint arXiv:2108.07258*, 2021.
- [30] Jared Kaplan, Sam McCandlish, Tom Henighan, Tom B Brown, Benjamin Chess, Rewon Child, Scott Gray, Alec Radford, Jeffrey Wu, and

Dario Amodei. Scaling laws for neural language models. *arXiv preprint arXiv:2001.08361*, 2020.

- [31] Alan L Hodgkin and Andrew F Huxley. A quantitative description of membrane current and its application to conduction and excitation in nerve. *The Journal of Physiology*, 117(4):500, 1952.
- [32] Larry F Abbott. Lapicque’s introduction of the integrate-and-fire model neuron (1907). *Brain Research Bulletin*, 50(5-6):303–304, 1999.
- [33] Eugene M Izhikevich. Simple model of spiking neurons. *IEEE Transactions on Neural Networks*, 14(6):1569–1572, 2003.
- [34] Bing Han, Gopalakrishnan Srinivasan, and Kaushik Roy. RMP-SNN: residual membrane potential neuron for enabling deeper high-accuracy and low-latency spiking neural network. In *2020 IEEE/CVF Conference on Computer Vision and Pattern Recognition, CVPR 2020, Seattle, WA, USA, June 13-19, 2020*, pages 13555–13564. Computer Vision Foundation / IEEE, 2020.
- [35] Tong Bu, Wei Fang, Jianhao Ding, Penglin Dai, Zhaofei Yu, and Tiejun Huang. Optimal ANN-SNN conversion for high-accuracy and ultra-low-latency spiking neural networks. In *The Tenth International Conference on Learning Representations, ICLR 2022, Virtual Event, April 25-29, 2022*. OpenReview.net, 2022.
- [36] Man Yao, Huanhuan Gao, Guangshe Zhao, Dingheng Wang, Yihan Lin, Zhaoxu Yang, and Guoqi Li. Temporal-wise attention spiking neural networks for event streams classification. In *Proceedings of the IEEE/CVF International Conference on Computer Vision*, pages 10221–10230, 2021.
- [37] Kexin Wang, Jiahong Zhang, Yong Ren, Man Yao, Di Shang, Bo Xu, and Guoqi Li. Spikevoice: High-quality text-to-speech via efficient spiking neural network. In Lun-Wei Ku, Andre Martins, and Vivek Srikumar, editors, *Proceedings of the 62nd Annual Meeting of the Association for Computational Linguistics (Volume 1: Long Papers), ACL 2024, Bangkok, Thailand, August 11-16, 2024*, pages 7927–7940. Association for Computational Linguistics, 2024.

- [38] Malyaban Bal and Abhroni Sengupta. Spikingbert: Distilling bert to train spiking language models using implicit differentiation. In *Proceedings of the AAAI Conference on Artificial Intelligence*, volume 38, pages 10998–11006, 2024.
- [39] Changze Lv, Yansen Wang, Dongqi Han, Xiaoqing Zheng, Xuanjing Huang, and Dongsheng Li. Efficient and effective time-series forecasting with spiking neural networks. In *Forty-first International Conference on Machine Learning, ICML 2024, Vienna, Austria, July 21-27, 2024*. OpenReview.net, 2024.
- [40] Won Jeon, Gun Ko, Jiwon Lee, Hyunwuk Lee, Dongho Ha, and Won Woo Ro. Deep learning with gpus. In *Advances in Computers*, volume 122, pages 167–215. Elsevier, 2021.
- [41] Sidi Yaya Arnaud Yarga and Sean UN Wood. Accelerating snn training with stochastic parallelizable spiking neurons. In *2023 International Joint Conference on Neural Networks (IJCNN)*, pages 1–8. IEEE, 2023.
- [42] Peng Xue, Wei Fang, Zhengyu Ma, Zihan Huang, Zhaokun Zhou, Yonghong Tian, Timothée Masquelier, and Huihui Zhou. Multiplication-free parallelizable spiking neurons with efficient spatio-temporal dynamics. In *The Thirty-ninth Annual Conference on Neural Information Processing Systems*, 2025.
- [43] Yulong Huang, Zunchang Liu, Changchun Feng, Xiaopeng Lin, Hongwei Ren, Haotian Fu, Yue Zhou, Hong Xing, and Bojun Cheng. Prf: Parallel resonate and fire neuron for long sequence learning in spiking neural networks. *arXiv preprint arXiv:2410.03530*, 2024.
- [44] Xinyi Chen, Jibin Wu, Chenxiang Ma, Yinsong Yan, Yujie Wu, and Kay Chen Tan. Pmsn: A parallel multi-compartment spiking neuron for multi-scale temporal processing. *arXiv preprint arXiv:2408.14917*, 2024.
- [45] Guobin Shen, Jindong Li, Tenglong Li, Dongcheng Zhao, and Yi Zeng. Spikepack: Enhanced information flow in spiking neural networks with high hardware compatibility. In *Proceedings of the IEEE/CVF International Conference on Computer Vision (ICCV)*, pages 23385–23395, October 2025.

- [46] Malyaban Bal and Abhroni Sengupta. P-spikessm: Harnessing probabilistic spiking state space models for long-range dependency tasks. In *The Thirteenth International Conference on Learning Representations, ICLR 2025, Singapore, April 24-28, 2025*. OpenReview.net, 2025.
- [47] Yan Zhong, Ruoyu Zhao, Chao Wang, Qinghai Guo, Jianguo Zhang, Zhichao Lu, and Liziwei Leng. Spike-ssm: A sparse, precise, and efficient spiking state space model for long sequences learning. *arXiv preprint arXiv:2410.17268*, 2024.
- [48] Wei Fang, Zhaofei Yu, Yanqi Chen, Timothée Masquelier, Tiejun Huang, and Yonghong Tian. Incorporating learnable membrane time constant to enhance learning of spiking neural networks. In *Proceedings of the IEEE/CVF International Conference on Computer Vision*, pages 2661–2671, 2021.
- [49] Adarsh Kumar Kosta and Kaushik Roy. Adaptive-spikenet: event-based optical flow estimation using spiking neural networks with learnable neuronal dynamics. In *2023 IEEE International Conference on Robotics and Automation (ICRA)*, pages 6021–6027. IEEE, 2023.
- [50] Cong Shi, Li Wang, Haoran Gao, and Min Tian. Learnable leakage and onset-spiking self-attention in snns with local error signals. *Sensors*, 23(24):9781, 2023.
- [51] Yongping Dan, Changhao Sun, Hengyi Li, and Lin Meng. Adaptive spiking neuron with population coding for a residual spiking neural network. *Applied Intelligence*, 55(4):288, 2025.
- [52] Tianqing Zhang, Kairong Yu, Jian Zhang, and Hongwei Wang. Da-lif: Dual adaptive leaky integrate-and-fire model for deep spiking neural networks. In *ICASSP 2025 - 2025 IEEE International Conference on Acoustics, Speech and Signal Processing (ICASSP)*, pages 1–5, 2025. doi: 10.1109/ICASSP49660.2025.10888909.
- [53] Yulong Huang, Xiaopeng Lin, Hongwei Ren, Haotian Fu, Yue Zhou, Zunchang Liu, Biao Pan, and Bojun Cheng. CLIF: Complementary leaky integrate-and-fire neuron for spiking neural networks. In Ruslan Salakhutdinov, Zico Kolter, Katherine Heller, Adrian Weller, Nuria Oliver, Jonathan Scarlett, and Felix Berkenkamp, editors, *Proceedings of*

the 41st International Conference on Machine Learning, volume 235 of *Proceedings of Machine Learning Research*, pages 19949–19972. PMLR, 21–27 Jul 2024.

- [54] Bojian Yin, Federico Corradi, and Sander M Bohté. Accurate and efficient time-domain classification with adaptive spiking recurrent neural networks. *Nature Machine Intelligence*, 3(10):905–913, 2021.
- [55] Alexandre Bittar and Philip N Garner. A surrogate gradient spiking baseline for speech command recognition. *Frontiers in Neuroscience*, 16: 865897, 2022.
- [56] Hanle Zheng, Zhong Zheng, Rui Hu, Bo Xiao, Yujie Wu, Fangwen Yu, Xue Liu, Guoqi Li, and Lei Deng. Temporal dendritic heterogeneity incorporated with spiking neural networks for learning multi-timescale dynamics. *Nature Communications*, 15(1):277, 2024.
- [57] Xingting Yao, Fanrong Li, Zitao Mo, and Jian Cheng. GLIF: A unified gated leaky integrate-and-fire neuron for spiking neural networks. In Sanmi Koyejo, S. Mohamed, A. Agarwal, Danielle Belgrave, K. Cho, and A. Oh, editors, *Advances in Neural Information Processing Systems 35: Annual Conference on Neural Information Processing Systems 2022, NeurIPS 2022, New Orleans, LA, USA, November 28 - December 9, 2022*, 2022.
- [58] Haoran Wang, Herui Zhang, Siyang Li, and Dongrui Wu. Gated parametric neuron for spike-based audio recognition. *Neurocomputing*, 609: 128477, 2024.
- [59] Jiqing Zhang, Malu Zhang, Yuanchen Wang, Qianhui Liu, Baocai Yin, Haizhou Li, and Xin Yang. Spiking neural networks with adaptive membrane time constant for event-based tracking. *IEEE Transactions on Image Processing*, 34:1009–1021, 2025. doi: 10.1109/TIP.2025.3533213.
- [60] Lihao Wang and Zhaofei Yu. Autaptic synaptic circuit enhances spatio-temporal predictive learning of spiking neural networks. In *Forty-first International Conference on Machine Learning, ICML 2024, Vienna, Austria, July 21-27, 2024*. OpenReview.net, 2024.
- [61] Liqun Luo. *Principles of neurobiology*. Garland Science, 2020.

- [62] Xinhao Luo, Man Yao, Yuhong Chou, Bo Xu, and Guoqi Li. Integer-valued training and spike-driven inference spiking neural network for high-performance and energy-efficient object detection. In *European Conference on Computer Vision*, pages 253–272. Springer, 2025.
- [63] Albert Gu and Tri Dao. Mamba: Linear-time sequence modeling with selective state spaces. In *First Conference on Language Modeling*, 2024.
- [64] Soham De, Samuel L Smith, Anushan Fernando, Aleksandar Botev, George Cristian-Muraru, Albert Gu, Ruba Haroun, Leonard Berrada, Yutian Chen, Srivatsan Srinivasan, et al. Griffin: Mixing gated linear recurrences with local attention for efficient language models. *arXiv preprint arXiv:2402.19427*, 2024.
- [65] Man Yao, Xuerui Qiu, Tianxiang Hu, Jiakui Hu, Yuhong Chou, Keyu Tian, Jianxing Liao, Luziwei Leng, Bo Xu, and Guoqi Li. Scaling spike-driven transformer with efficient spike firing approximation training. *IEEE Transactions on Pattern Analysis and Machine Intelligence*, 47(4): 2973–2990, 2025.
- [66] Songlin Yang, Bailin Wang, Yikang Shen, Rameswar Panda, and Yoon Kim. Gated linear attention transformers with hardware-efficient training. In *Forty-first International Conference on Machine Learning, ICML 2024, Vienna, Austria, July 21-27, 2024*. OpenReview.net, 2024.
- [67] Eric Martin and Chris Cundy. Parallelizing linear recurrent neural nets over sequence length. In *6th International Conference on Learning Representations, ICLR 2018, Vancouver, BC, Canada, April 30 - May 3, 2018, Conference Track Proceedings*. OpenReview.net, 2018.
- [68] Philippe Tillet, Hsiang-Tsung Kung, and David Cox. Triton: an intermediate language and compiler for tiled neural network computations. In *Proceedings of the 3rd ACM SIGPLAN International Workshop on Machine Learning and Programming Languages*, pages 10–19, 2019.
- [69] Songlin Yang and Yu Zhang. Fla: A triton-based library for hardware-efficient implementations of linear attention mechanism, January 2024. URL <https://github.com/fla-org/flash-linear-attention>.
- [70] Stephen Merity, Caiming Xiong, James Bradbury, and Richard Socher. Pointer sentinel mixture models. In *5th International Conference on*

Learning Representations, ICLR 2017, Toulon, France, April 24-26, 2017, Conference Track Proceedings. OpenReview.net, 2017.

- [71] Yufei Guo, Yuhang Zhang, Yuanpei Chen, Weihang Peng, Xiaode Liu, Liwen Zhang, Xuhui Huang, and Zhe Ma. Membrane potential batch normalization for spiking neural networks. In *IEEE/CVF International Conference on Computer Vision, ICCV 2023, Paris, France, October 1-6, 2023*, pages 19363–19373. IEEE, 2023. doi: 10.1109/ICCV51070.2023.01779.
- [72] Yufei Guo, Yuanpei Chen, Liwen Zhang, YingLei Wang, Xiaode Liu, Xinyi Tong, Yuanyuan Ou, Xuhui Huang, and Zhe Ma. Reducing information loss for spiking neural networks. In Shai Avidan, Gabriel Brostow, Moustapha Cissé, Giovanni Maria Farinella, and Tal Hassner, editors, *Computer Vision – ECCV 2022*, pages 36–52, Cham, 2022. Springer Nature Switzerland. ISBN 978-3-031-20083-0.
- [73] Wei Liu, Li Yang, Mingxuan Zhao, Shuxun Wang, Jin Gao, Wenjuan Li, Bing Li, and Weiming Hu. Deeptage: Deep temporal-aligned gradient enhancement for optimizing spiking neural networks. In *The Thirteenth International Conference on Learning Representations, ICLR 2025, Singapore, April 24-28, 2025*. OpenReview.net, 2025.
- [74] A. Krizhevsky and G. Hinton. Learning multiple layers of features from tiny images. *Handbook of Systemic Autoimmune Diseases*, 1, 2009.
- [75] Jia Deng, Wei Dong, Richard Socher, Li-Jia Li, Kai Li, and Li Fei-Fei. Imagenet: A large-scale hierarchical image database. In *2009 IEEE Computer Society Conference on Computer Vision and Pattern Recognition (CVPR 2009), 20-25 June 2009, Miami, Florida, USA*, pages 248–255. IEEE Computer Society, 2009. doi: 10.1109/CVPR.2009.5206848.
- [76] Hongmin Li, Hanchao Liu, Xiangyang Ji, Guoqi Li, and Luping Shi. Cifar10-dvs: An event-stream dataset for object classification. *Frontiers in Neuroscience*, Volume 11 - 2017, 2017. ISSN 1662-453X. doi: 10.3389/fnins.2017.00309.
- [77] Shikuang Deng, Yuhang Li, Shanghang Zhang, and Shi Gu. Temporal efficient training of spiking neural network via gradient re-weighting. In

The Tenth International Conference on Learning Representations, ICLR 2022, Virtual Event, April 25-29, 2022. OpenReview.net, 2022.

- [78] Yaguang Li, Rose Yu, Cyrus Shahabi, and Yan Liu. Diffusion convolutional recurrent neural network: Data-driven traffic forecasting. In *6th International Conference on Learning Representations, ICLR 2018, Vancouver, BC, Canada, April 30 - May 3, 2018, Conference Track Proceedings*. OpenReview.net, 2018.
- [79] Guokun Lai, Wei-Cheng Chang, Yiming Yang, and Hanxiao Liu. Modeling long-and short-term temporal patterns with deep neural networks. In *The 41st international ACM SIGIR conference on research & development in information retrieval*, pages 95–104, 2018.
- [80] Ashish Vaswani, Noam Shazeer, Niki Parmar, Jakob Uszkoreit, Llion Jones, Aidan N. Gomez, Łukasz Kaiser, and Illia Polosukhin. Attention is all you need. In Isabelle Guyon, Ulrike von Luxburg, Samy Bengio, Hanna M. Wallach, Rob Fergus, S. V. N. Vishwanathan, and Roman Garnett, editors, *Advances in Neural Information Processing Systems 30: Annual Conference on Neural Information Processing Systems 2017, December 4-9, 2017, Long Beach, CA, USA*, pages 5998–6008, 2017.
- [81] Yong Liu, Tengge Hu, Haoran Zhang, Haixu Wu, Shiyu Wang, Lintao Ma, and Mingsheng Long. itransformer: Inverted transformers are effective for time series forecasting. In *The Twelfth International Conference on Learning Representations, ICLR 2024, Vienna, Austria, May 7-11, 2024*. OpenReview.net, 2024.
- [82] Tong Bu, Maohua Li, and Zhaofei Yu. Inference-scale complexity in ann-snn conversion for high-performance and low-power applications. In *Proceedings of the Computer Vision and Pattern Recognition Conference*, pages 24387–24397, 2025.
- [83] Guangzhi Tang, Neelesh Kumar, Raymond Yoo, and Konstantinos Michmizos. Deep reinforcement learning with population-coded spiking neural network for continuous control. In *Conference on Robot Learning*, pages 2016–2029. PMLR, 2021.
- [84] Duzhen Zhang, Tielin Zhang, Shuncheng Jia, and Bo Xu. Multi-sacle dynamic coding improved spiking actor network for reinforcement learn-

ing. In *Proceedings of the AAAI Conference on Artificial Intelligence*, volume 36, pages 59–67, 2022.

- [85] Ding Chen, Peixi Peng, Tiejun Huang, and Yonghong Tian. Fully spiking actor network with intralayer connections for reinforcement learning. *IEEE Transactions on Neural Networks and Learning Systems*, 36(2):2881–2893, 2024.
- [86] Zijie Xu, Tong Bu, Zecheng Hao, Jianhao Ding, and Zhaofei Yu. Proxy target: Bridging the gap between discrete spiking neural networks and continuous control. In *The Thirty-ninth Annual Conference on Neural Information Processing Systems*, 2025.
- [87] Emanuel Todorov. Convex and analytically-invertible dynamics with contacts and constraints: Theory and implementation in mujoco. In *2014 IEEE International Conference on Robotics and Automation (ICRA)*, pages 6054–6061. IEEE, 2014.
- [88] Tom Erez, Yuval Tassa, and Emanuel Todorov. Infinite-horizon model predictive control for periodic tasks with contacts. In *Robotics: Science and systems*, volume 7, page 73, 2012.
- [89] Rui-Jie Zhu, Qihang Zhao, Guoqi Li, and Jason Eshraghian. Spikegpt: Generative pre-trained language model with spiking neural networks. *Trans. Mach. Learn. Res.*, 2024, 2024.
- [90] Albert Gu, Karan Goel, and Christopher Ré. Efficiently modeling long sequences with structured state spaces. In *The Tenth International Conference on Learning Representations, ICLR 2022, Virtual Event, April 25-29, 2022*. OpenReview.net, 2022.
- [91] Shuming Ma, Hongyu Wang, Lingxiao Ma, Lei Wang, Wenhui Wang, Shaohan Huang, Li Dong, Ruiping Wang, Jilong Xue, and Furu Wei. The era of 1-bit llms: All large language models are in 1.58 bits. *arXiv preprint arXiv:2402.17764*, 2024.
- [92] Rui-Jie Zhu, Yu Zhang, Ethan Sifferman, Tyler Sheaves, Yiqiao Wang, Dustin Richmond, Peng Zhou, and Jason K Eshraghian. Scalable matmul-free language modeling. *arXiv preprint arXiv:2406.02528*, 2024.

- [93] Kaiwen Tang, Zhanglu Yan, and Weng-Fai Wong. Sorbet: A neuromorphic hardware-compatible transformer-based spiking language model. In *Forty-second International Conference on Machine Learning, ICML 2025, Vancouver, Canada, July 13-19, 2025*, 2025.
- [94] Ilya Loshchilov and Frank Hutter. Decoupled weight decay regularization. In *7th International Conference on Learning Representations, ICLR 2019, New Orleans, LA, USA, May 6-9, 2019*. OpenReview.net, 2019.
- [95] Jason K. Eshraghian, Max Ward, Emre O. Neftci, Xinxin Wang, Gregor Lenz, Girish Dwivedi, Mohammed Bennamoun, Doo Seok Jeong, and Wei D. Lu. Training spiking neural networks using lessons from deep learning. *Proc. IEEE*, 111(9):1016–1054, 2023.
- [96] Wei Fang, Yanqi Chen, Jianhao Ding, Zhaofei Yu, Timothée Masquelier, Ding Chen, Liwei Huang, Huihui Zhou, Guoqi Li, and Yonghong Tian. Spikingjelly: An open-source machine learning infrastructure platform for spike-based intelligence. *Science Advances*, 9(40):eadi1480, 2023.
- [97] Diederik P. Kingma and Jimmy Ba. Adam: A method for stochastic optimization. In Yoshua Bengio and Yann LeCun, editors, *3rd International Conference on Learning Representations, ICLR 2015, San Diego, CA, USA, May 7-9, 2015, Conference Track Proceedings*, 2015.
- [98] Haoran You, Xiaohan Chen, Yongan Zhang, Chaojian Li, Sicheng Li, Zihao Liu, Zhangyang Wang, and Yingyan Lin. Shiftaddnet: A hardware-inspired deep network. *Advances in Neural Information Processing Systems*, 33:2771–2783, 2020.

Appendix A. Details of Theoretical Analysis

Appendix A.1. Control Ability over Membrane Potential of Reset

In this section, building on the definitions of Δ -short control and long control presented in the main text, we conduct a more rigorous analysis of how the reset mechanism in vanilla spiking neurons controls the membrane potential, which helps us understand its limitations.

Similar to LIF neurons, the charging equation for IF neurons can be written as:

$$H_t = H_{t-1} + X_t \quad (\text{A.1})$$

We combine the Eq. 3 and Eq. A.1, and derive one-step iteration of the membrane potential:

$$H_t = \begin{cases} (1 - f(H_{t-1}))H_{t-1} + X_t, & \text{hard reset} \\ H_{t-1} - V_{\text{th}}f(H_{t-1}) + X_t, & \text{soft reset} \end{cases} \quad (\text{A.2})$$

Where f is the firing function. $f(H_t) = 1$ when $H_t \geq V_{\text{th}}$; otherwise $f(H_t) = 0$. With these prerequisites established, we discuss whether IF and LIF neurons strictly possess Δ -short and long control abilities over the membrane potential under hard reset or soft reset conditions.

Proposition Appendix A.1. *Hard reset in IF neurons has both Δ -short and long control abilities over the membrane potential.*

Proof. Firstly, suppose $H_{t-\Delta} \geq V_{\text{th}}$ and $X_{t-\Delta+1}, \dots, X_t < V_{\text{th}}/\Delta$, then

$$\begin{aligned} H_{t-\Delta+1} &= 0 + X_{t-\Delta+1} < V_{\text{th}}/\Delta \\ H_{t-\Delta+2} &= H_{t-\Delta+1} + X_{t-\Delta+2} < V_{\text{th}}/\Delta + V_{\text{th}}/\Delta = 2V_{\text{th}}/\Delta \\ H_{t-\Delta+3} &= H_{t-\Delta+2} + X_{t-\Delta+3} < 2V_{\text{th}}/\Delta + V_{\text{th}}/\Delta = 3V_{\text{th}}/\Delta \\ &\dots \\ H_{t-\Delta+\Delta} &= H_{t-\Delta+\Delta-1} + X_{t-\Delta+\Delta} < (\Delta - 1)V_{\text{th}}/\Delta + V_{\text{th}}/\Delta = V_{\text{th}} \end{aligned} \quad (\text{A.3})$$

Thus, we obtain $H_t < V_{\text{th}}$.

Secondly, suppose $X_i \leq C, i = 1, \dots, t$. It is easy to get that $H_1 = X_1 <$

$C + V_{\text{th}}$. Besides, if $H_{t-1} < C + V_{\text{th}}$, then

$$\begin{aligned} H_t &= (1 - f(H_{t-1}))H_{t-1} + X_t \\ &= \begin{cases} H_{t-1} + X_t < C + V_{\text{th}}, & H_{t-1} < V_{\text{th}} \\ X_t < C + V_{\text{th}}, & V_{\text{th}} \leq H_{t-1} < C + V_{\text{th}} \end{cases} \end{aligned} \quad (\text{A.4})$$

By mathematical induction, we know that $\{H_t\}$ has an upper bound $C + V_{\text{th}}$.

From Definition 3.2 and 3.3, IF with hard reset has both Δ -short and long control abilities. \square

Proposition Appendix A.2. *Hard reset in LIF neurons has both Δ -short and long control abilities over the membrane potential.*

Proof. Firstly, suppose $H_{t-\Delta} \geq V_{\text{th}}$ and $X_{t-\Delta+1}, \dots, X_t < V_{\text{th}}/\Delta$, then

$$\begin{aligned} H_{t-\Delta+1} &= 0 + (1 - \beta)X_{t-\Delta+1} < V_{\text{th}}/\Delta \\ H_{t-\Delta+2} &= \beta H_{t-\Delta+1} + (1 - \beta)X_{t-\Delta+2} < V_{\text{th}}/\Delta + V_{\text{th}}/\Delta = 2V_{\text{th}}/\Delta \\ H_{t-\Delta+3} &= \beta H_{t-\Delta+2} + (1 - \beta)X_{t-\Delta+3} < 2V_{\text{th}}/\Delta + V_{\text{th}}/\Delta = 3V_{\text{th}}/\Delta \\ &\dots \\ H_{t-\Delta+\Delta} &= \beta H_{t-\Delta+\Delta-1} + (1 - \beta)X_{t-\Delta+\Delta} < (\Delta - 1)V_{\text{th}}/\Delta + V_{\text{th}}/\Delta = V_{\text{th}} \end{aligned} \quad (\text{A.5})$$

Thus, we obtain $H_t < V_{\text{th}}$.

Secondly, suppose $X_i \leq C, i = 1, \dots, t$. It is easy to get that $H_1 = (1 - \beta)X_1 \leq C$. Besides, if $H_{t-1} \leq C$, then

$$H_t = \beta(1 - f(H_{t-1}))H_{t-1} + (1 - \beta)X_t \leq \beta C + (1 - \beta)C = C \quad (\text{A.6})$$

By mathematical induction, we know that $\{H_t\}$ has an upper bound C .

From Definition 3.2 and 3.3, LIF with hard reset has both Δ -short and long control abilities. \square

Remark: Hard reset immediately clears the membrane potential at the current timestep. However, regardless of input magnitude, its effect lasts only one timestep and cannot adaptively adjust its range. Therefore, although hard reset possesses the ability of Δ -short control, its actual control window collapses to a fixed value of $\Delta = 1$.

We next turn to soft reset, which controls the membrane potential by subtracting a fixed value. We will show that, due to its lack of flexibility,

soft reset is also not an effective mechanism for controlling the membrane potential. Before that, we introduce a lemma needed for the formal proof.

Lemma Appendix A.1. *For any positive integer Δ and any positive integer $m \leq \Delta$, we have*

$$\Delta + \frac{m}{\Delta} - m \geq 1 \quad (\text{A.7})$$

Proof. When $m = \Delta$, the equality holds.

When $1 \leq m < \Delta$, consider the function

$$f(x) = \Delta + \frac{x}{\Delta} - x = \left(\frac{1}{\Delta} - 1\right)x + \Delta, \quad x \in [1, \Delta], \Delta > 1. \quad (\text{A.8})$$

Since $f(x)$ is monotonically decreasing in x , $f(m) > f(\Delta) = \Delta + 1 - \Delta = 1$. \square

Proposition Appendix A.3. *Soft reset in IF neurons has neither Δ -short nor long control abilities over the membrane potential.*

Proof. Firstly, suppose $H_{t-\Delta} \geq V_{\text{th}}$ and $X_{t-\Delta+1}, \dots, X_t < V_{\text{th}}/\Delta$. If $H_{t-\Delta} > (\Delta + 1)V_{\text{th}} - \sum_{i=1}^{\Delta} X_{t-\Delta+i} > V_{\text{th}}$, then, in combination with Lemma Appendix A.1, we have

$$\begin{aligned} H_{t-\Delta+1} &= H_{t-\Delta} - V_{\text{th}} + X_{t-\Delta+1} \\ &> \Delta \cdot V_{\text{th}} - \sum_{i=2}^{\Delta} X_{t-\Delta+i} > \left(\Delta + \frac{1}{\Delta} - 1\right)V_{\text{th}} \geq V_{\text{th}} \\ H_{t-\Delta+2} &= H_{t-\Delta+1} - V_{\text{th}} + X_{t-\Delta+2} \\ &> (\Delta - 1)V_{\text{th}} - \sum_{i=3}^{\Delta} X_{t-\Delta+i} > \left(\Delta + \frac{2}{\Delta} - 2\right)V_{\text{th}} \geq V_{\text{th}} \quad (\text{A.9}) \\ &\dots \\ H_{t-\Delta+\Delta-1} &= H_{t-\Delta+\Delta-2} - V_{\text{th}} + X_{t-\Delta+\Delta-1} \\ &> 2V_{\text{th}} - X_t > \left(\Delta + \frac{\Delta-1}{\Delta} - (\Delta - 1)\right)V_{\text{th}} \geq V_{\text{th}} \\ H_{t-\Delta+\Delta} &= H_{t-\Delta+\Delta-1} - V_{\text{th}} + X_{t-\Delta+\Delta} > V_{\text{th}} \end{aligned}$$

Thus, we obtain $H_t > V_{\text{th}}$. From Definition 3.2, Δ -short control ability does not hold in this case.

Secondly, let $X_i = C > V_{\text{th}}, i = 1, \dots, t$. For any $C_H > V_{\text{th}}$, there exists $t_0 \geq \frac{C_H - V_{\text{th}}}{C - V_{\text{th}}}$ such that when $t > t_0$,

$$\begin{aligned} H_t &= H_{t-1} - V_{\text{th}} + X_t \\ &= H_{t-2} + (X_{t-1} + X_t) - 2V_{\text{th}} = \dots \\ &= \sum_{i=1}^t X_i - (t-1)V_{\text{th}} \\ &= tC - (t-1)V_{\text{th}} > C_H \end{aligned} \tag{A.10}$$

In this case, $\{H_t\}$ does not have an upper bound. From Definition 3.3, long control ability does not hold. \square

Proposition Appendix A.4. *Soft reset in LIF neurons does not have Δ -short control, but has long control ability over the membrane potential.*

Proof. Firstly, suppose $H_{t-\Delta} \geq V_{\text{th}}$ and $X_{t-\Delta+1}, \dots, X_t < V_{\text{th}}/\Delta$. To make Δ -short control fail, it suffices to have $H_t = \beta(H_{t-1} - V_{\text{th}}) + (1 - \beta)X_t \geq V_{\text{th}}$, which requires

$$H_{t-1} \geq (1 + \frac{1}{\beta})V_{\text{th}} + (1 - \frac{1}{\beta})X_t \tag{A.11}$$

Since $H_{t-1} = \beta(H_{t-2} - V_{\text{th}}) + (1 - \beta)X_{t-1}$, this implies

$$H_{t-2} \geq (1 + \frac{1}{\beta} + \frac{1}{\beta^2})V_{\text{th}} + (1 - \frac{1}{\beta})X_{t-1} + \frac{1}{\beta}(1 - \frac{1}{\beta})X_t \tag{A.12}$$

By recursion, we need

$$H_{t-\Delta} \geq \sum_{i=0}^{\Delta} \frac{1}{\beta^i} V_{\text{th}} + \sum_{i=1}^{\Delta} \frac{1}{\beta^{i-1}} (1 - \frac{1}{\beta}) X_{t-\Delta+i} \tag{A.13}$$

From Definition 3.2, Δ -short control ability does not hold in this case.

Secondly, suppose $X_i \leq C, i = 1, \dots, t$. It is easy to get that $H_1 = (1 - \beta)X_1 \leq C$. Besides, if $H_{t-1} \leq C$, then

$$H_t = \beta(H_{t-1} - V_{\text{th}}f(H_{t-1})) + (1 - \beta)X_t \leq \beta C + (1 - \beta)C = C \tag{A.14}$$

By mathematical induction, we know that $\{H_t\}$ has an upper bound C . From Definition 3.3, long control ability holds. \square

Remark: In soft reset, for any given upper bound Δ on the control window, there always exists a sufficiently large input that extends its effect beyond this bound, leading to continuous spike firing. Moreover, the subtracted value is fixed, while the accumulation of the membrane potential varies dynamically. When the accumulation rate exceeds the subtraction rate, the membrane potential may explode even with soft reset mechanism. This situation can only be prevented by introducing an additional leakage factor β .

Appendix A.2. Proof of Functions of Dynamic Decay

Proposition Appendix A.5. *Dynamic decay can introduce nonlinearity and enabling more flexible Δ -short and long control of the membrane potential than the reset mechanism.*

Proof. Firstly, with dynamic decay, the iteration form of the membrane potential is:

$$H_t = \alpha_t H_{t-1} + (1 - \alpha_t) X_t. \quad (\text{A.15})$$

which can be rewritten as

$$H_t = \sum_{i=1}^t \left(\prod_{j=i+1}^t \alpha_j \right) (1 - \alpha_i) X_i. \quad (\text{A.16})$$

Note that the coefficient of X_i is input-dependent, which implies that the combination of X_i is not actually a linear term. From Definition 3.1, we conclude that dynamic decay introduces nonlinearity.

Next, we show how α_t controls the membrane potential H_t . Given $\Delta \in \mathbb{N}^+$, suppose $H_{t-\Delta} \geq V_{\text{th}}$ and $X_{t-\Delta+1}, \dots, X_t < V_{\text{th}}/\Delta$. Note that when

$$\alpha_{t-\Delta+1} < \frac{V_{\text{th}} - X_{t-\Delta+1}}{H_{t-\Delta} - X_{t-\Delta+1}} \in (0, 1] \quad (\text{A.17})$$

We have

$$\begin{aligned} H_{t-\Delta+1} &= \alpha_{t-\Delta+1} H_{t-\Delta} + (1 - \alpha_{t-\Delta+1}) X_{t-\Delta+1} \\ &= \alpha_{t-\Delta+1} (H_{t-\Delta} - X_{t-\Delta+1}) + X_{t-\Delta+1} \\ &< V_{\text{th}} - X_{t-\Delta+1} + X_{t-\Delta+1} = V_{\text{th}}. \end{aligned} \quad (\text{A.18})$$

For $m = 2, 3, \dots, \Delta$, we sequentially derive

$$\begin{aligned} H_{t-\Delta+m} &= \alpha_{t-\Delta+m} H_{t-\Delta+m-1} + (1 - \alpha_{t-\Delta+m}) X_{t-\Delta+m} \\ &< \alpha_{t-\Delta+m} V_{\text{th}} + (1 - \alpha_{t-\Delta+m}) V_{\text{th}} = V_{\text{th}} \end{aligned} \quad (\text{A.19})$$

When $m = \Delta$, $H_t < V_{\text{th}}$. From Definition 3.2, every α_t satisfying Eq. A.17 can guarantee Δ -short control ability and avert continuous firing when inputs are smaller than threshold.

For long control ability, suppose that $\{X_t\}$ has an upper bound C , i.e., $X_i \leq C, i = 1, 2, \dots, t$. It is easy to get that $H_1 = (1 - \alpha_1)X_1 \leq C$. Besides, if $H_{t-1} \leq C$, then

$$H_t = \alpha_t H_{t-1} + (1 - \alpha_t) X_t \leq \alpha_t C + (1 - \alpha_t) C = C \quad (\text{A.20})$$

By mathematical induction, we know that $\{H_t\}$ has an upper bound C . From Definition 3.3, α_t has long control ability. \square

Remark: Dynamic decay surpasses the reset mechanism in both introducing nonlinearity and controlling the membrane potential. On one hand, the nonlinearity of dynamic decay is governed by the input-dependent coefficient α_t , which can theoretically vary freely within $[0,1]$. In contrast, the nonlinearity in the reset mechanism is discrete and limited (either a complete reset to zero or a fixed subtraction). On the other hand, dynamic decay provides more flexible control over the membrane potential. In particular, regarding Δ -short control, it allows a defined upper bound Δ for an arbitrarily large membrane potential, while enabling the actual duration of influence within this window to adapt dynamically based on the input. In the above proof, we derived the condition under which a large membrane potential has an effective duration of 1 (Eq. A.17). In fact, we can further generalize this result to obtain the condition for an actual duration of $\tau \in [1, \Delta]$:

$$\begin{cases} \alpha_{t-\Delta+i} \geq \frac{V_{\text{th}} - X_{t-\Delta+i}}{H_{t-\Delta+i-1} - X_{t-\Delta+i}}, & i = 1, 2, \dots, \tau - 1 \\ \alpha_{t-\Delta+i} < \frac{V_{\text{th}} - X_{t-\Delta+i}}{H_{t-\Delta+i-1} - X_{t-\Delta+i}}, & i = \tau \end{cases} . \quad (\text{A.21})$$

In this case, $H_{t-\Delta}, H_{t-\Delta+1}, \dots, H_{t-\Delta+\tau-1} \geq V_{\text{th}}$ and $H_{t-\Delta}$ triggers a total of τ spikes.

Appendix A.3. Dynamic Decay in Integer-valued Training Case

When the integer-valued training technique is introduced, dynamic decay is still able to retain the two functions of the reset mechanism. According to Proposition 1 of [65], integer-value output (with upper bound N) is equal to the sum of spikes generated by IF-SR (IF with Soft Reset) spiking neuron with N timesteps. Therefore, functions of the reset mechanism are still preserved at the single-neuron level. Consequently, Proposition 4.1 should still hold in the integer spike scenario.

In fact, assuming the integer spiking function $f(H_t) = \lfloor \text{Clip}(H_t, 0, N) \rfloor$ and $V_{\text{th}} = 1$, where $\text{Clip}(x, 0, N)$ means clipping the input x to the range $[0, N]$, and $\lfloor \cdot \rfloor$ is the floor function. Since the functions of non-linearity and membrane potential control in dynamic decay are independent of the choice of the spike firing function, this concludes our functional analysis in Proposition 4.1 in integer-valued training case.

Appendix B. Experimental Details

In this work, we set DSN hyperparameters $N = 4$, $k = 4$, and $\tau = 0.25$. The dynamic decay form of DSN matches the HGRN operator in flash-linear-attention library². Therefore, in this paper, we leverage this Triton operator to enable parallel training of DSN.

Appendix B.1. Training Efficiency and Extrapolation

Training Efficiency. We evaluate the training efficiency of different parallelizable spiking neurons by measuring the average runtime of 100 forward and backward passes under sequence lengths from 2k to 16k. We set the batch size processed by the spiking neurons to 16 and the number of spiking neurons to 512. For sliding PSN [1], we set the sliding window $k = 64$.

Extrapolation. We conduct experiments on WikiText-103 [70] dataset using SpikingSSM [27] architecture with different spiking neurons. Models are trained on sequences of length 2k and evaluated on sequences of length 1k to 30k. During the testing phase, to allow the construction of sufficiently long sequences on the test set, we set the batch size to 1. The remaining experimental settings follow Appendix B.5. For masked PSN [1], We align the order k with the training length. For sliding PSN [1], we set the sliding window $k = 32$.

²<https://github.com/fla-org/flash-linear-attention>

Appendix B.2. Sequential CIFAR, ImageNet and CIFAR10-DVS

Sequential CIFAR. We use the width of the image as the sequence length ($L = 32$) to obtain a serialized version of CIFAR dataset. The model architecture is consistent with that of PSN [1] as detailed in Table B.10. For hyperparameter settings, the training is conducted over 256 epochs with a cosine decay learning rate schedule, starting at a maximum of 0.001. We set the batch size to 128 and select AdamW optimizer [94] with zero weight decay.

Table B.10: Configurations of Conv-based SNNs for Sequential CIFAR dataset. BN: BatchNorm, FC: Fully Connected.

Stage	Layer Specification	Configuration
1	Conv1D-BN-DSN Block $\times 3$	Conv: (3, stride=1, padding=1), Dim: 128
	Average Pooling	Feature size: 32 \rightarrow 16
2	Conv1D-BN-DSN Block $\times 3$	Conv: (3, stride=1, padding=1), Dim: 128
	Average Pooling	Feature size: 16 \rightarrow 8
3	Flatten-FC1-DSN-FC2	FC1: 1024 \rightarrow 256, FC2: 256 \rightarrow class_num

ImageNet and CIFAR10-DVS. For ImageNet, our experimental setup is identical to that of PSN [1]. For CIFAR10-DVS, we use AdamW [94] as the optimizer with a learning rate of 0.001, while keeping all other settings consistent with PSN.

Appendix B.3. Time-series Forcasting Tasks

We rely on SnnTorch [95] and SpikingJelly [96] to build the baseline networks. For SNNs with LIF neurons, we set the training timestep $T = 4$, the threshold $V_{\text{th}} = 1.0$, and the decay rate $\beta = 0.99$. For SNNs with DSN neurons, thanks to integer-valued training techniques, we do not directly expand timesteps to perform 0-1 encoding for temporal tasks. Instead, $N = 4$ is regarded as the expanded 4 timesteps. The architecture and size of DSN-based model are aligned with [39]. For training hyperparameters, we use a batch size of 128 and employ Adam optimizer [97] with a learning rate of 1×10^{-4} . An early stopping strategy is implemented with a tolerance of 30 epochs. The experiments are conducted using 4 NVIDIA RTX A6000 GPUs.

To assess the performance of our model, we use the Root Relative Squared Error (RSE) and the coefficient of determination (R^2), defined as follows:

$$RSE = \sqrt{\frac{\sum_{m=1}^M \|\mathbf{Y}^m - \hat{\mathbf{Y}}^m\|^2}{\sum_{m=1}^M \|\mathbf{Y}^m - \bar{\mathbf{Y}}\|^2}}, \quad (B.1)$$

$$R^2 = \frac{1}{MCL} \sum_{m=1}^M \sum_{c=1}^C \sum_{l=1}^L \left[1 - \frac{(Y_{c,l}^m - \hat{Y}_{c,l}^m)^2}{(Y_{c,l}^m - \bar{Y}_{c,l})^2} \right]. \quad (B.2)$$

In these formulas, M is the size of the test set, C is the number of channels, and L is the prediction length. $\bar{\mathbf{Y}}$ represents the average of \mathbf{Y}^m . $Y_{c,l}^m$ denotes the l -th future value of the c -th variable in the m -th sample, while $\bar{Y}_{c,l}$ is its average across all samples. $\hat{\mathbf{Y}}^m$ and $\hat{Y}_{c,l}^m$ denote the ground truth values. Unlike Mean Squared Error (MSE) or Mean Absolute Error (MAE), these metrics are less sensitive to the absolute scale of the dataset, making them particularly well suited for time-series forecasting tasks.

Regarding the improvements in Spikformer [12], in addition to replacing the spiking neurons, we also make architectural modifications to achieve better performance. Specifically, we expand the first DSN in the Feed-Forward Network (FFN) block to an enhanced DSN mentioned in Sec. 4 to improve the interaction between different neuron channels. However, this increases the total number of parameters in the FFN block by $16C^2$, where C is the number of channels. To maintain the same total parameter count $8C^2$ of the FFN block, we reduce the expansion ratio of the linear mapping from the usual 4 to 2. The architecture of the FFN block before and after modification is shown in Fig. B.6.

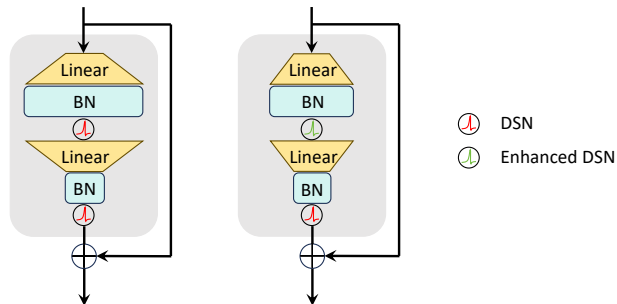


Figure B.6: The FFN block in Spikformer with DSN before (left) and after (right) modification. BN: BatchNorm.

Appendix B.4. Reinforcement Learning

Baseline results are reproduced by strictly following the protocol of Xu et al. [86]. All results are reported as the maximum average return over five random seeds. For fair comparison, SNN models with DSN neurons share the same architecture as the PT-LIF models in Xu et al. [86], and all experiments are conducted using the configurations released in the official implementation on Github³.

Appendix B.5. WikiText-103

Our experiment is implemented on 8 NVIDIA A800 GPUs. The network architecture and hyperparameters are largely based on S4 [90] and SpikingSSM [27], as shown in Table B.11. The key difference is that we shorten the length of the training text to 2048. To maintain the number of tokens per training step, we increase the batch size per GPU to 4.

Table B.11: Configurations of DSN-based language model on WikiText-103.

Configurations	WikiText-103
Layer Depth	16
Model Dimension	1024
Learning Rate	5e-4
Learning Rate Schedule	Cosine Decay, with 500 warmup steps
Optimizer	AdamW [94]
Weight Decay	0.01
Batch Size per GPU	8
Epochs	100

Appendix B.6. Analysis of Energy Consumption

We follow the method in [13] to evaluate the energy consumption of the Sequential CIFAR network using different spiking neurons. Specifically, the energy consumption for floating-point operations (FLOPs) is calculated by $E_{MAC} \cdot FLOPs$, while the energy consumption for spike-based operations is calculated by $E_{AC} \cdot T \cdot R \cdot FLOPs$. Here, $E_{MAC} = 4.6pJ$ and $E_{AC} = 0.9pJ$

³<https://github.com/xuzijie32/Proxy-Target>

Table B.12: Statistical methods of FLOPs within spiking neurons. c : number of spiking neuron. T : Timestep. k : kernel size of causal convolution.

Spiking Neuron	Internal Structure	FLOPs
LIF [32]	Update of Membrane Potential	$c \cdot T$
PSN [1]	Update of Membrane Potential	$c \cdot T^2$
sliding PSN [1]	Update of Membrane Potential	$0.5c \cdot T^2$
DSN (Ours)	Causal Conv1D	$k \cdot c \cdot T$
	Sigmoid Function	$c \cdot T$
	Update of Membrane Potential	$c \cdot T$

in 45nm technology. T denotes timestep and R denotes the spike firing rate. The FLOPs of the n -th Conv1D layer are $k_n \cdot d_n \cdot c_{n-1} \cdot c_n$, where k_n is the kernel size, d_n is the sequence channel number, c_{n-1} and c_n are the input and output convolution channel numbers, respectively. The FLOPs of the m -th fully connected layer are $i_m \cdot o_m$, where i_m and o_m are the input and output channels of the layers.

According to [93], the Sigmoid function can be implemented using two shift operations and one addition. We scaled the energy consumption of shift operations reported in [98] proportionally to a 45nm technology, yielding an energy cost of $0.72pJ$ per shift. Therefore, the energy consumption of a single sigmoid computation can be reduced to $2 * 0.72 + 0.9 = 2.34pJ$.

The energy consumption from LIF neurons itself is usually considered negligible compared to that of the network architecture, including convolution and fully connected layers. In contrast, PSN and DSN have more complex internal structures, leading to non-negligible energy consumption. To ensure fairness, we present a statistical method for FLOPs within spiking neurons and summarize it in Table B.12.

The spike firing rates of different layers⁴ in Conv-based SNN for Sequential CIFAR using different spiking neurons are presented in Table B.13. Our DSN exhibits a lower spike firing rate than that of LIF, which helps offset the additional energy cost introduced by the dynamic decay module.

⁴Notably, the input to the first convolutional layer are floating-point numbers of the original sequence, rather than processed spikes. Therefore, this layer is not involved in the calculation of the spike firing rate.

Table B.13: Spike firing rates of Conv-based SNN for Sequential CIFAR10 and CIFAR100. Conv x : Conv1D of the x -th layer. FC: Fully Connected.

Dataset	Methods	Conv2	Conv3	Conv4	Conv5	Conv6	FC1	FC2	Average
Sequential CIFAR10	LIF [32]	0.1511	0.1422	0.1811	0.1553	0.1457	0.0926	0.0647	0.1499
	PSN [1]	0.2200	0.3101	0.1575	0.1542	0.1516	0.1439	0.1239	0.2143
	sliding PSN [1]	0.1792	0.1875	0.1297	0.2538	0.1923	0.0764	0.1172	0.1820
	DSN (Ours)	0.1349	0.1337	0.1301	0.1301	0.0982	0.0380	0.0484	0.1238
Sequential CIFAR100	LIF [32]	0.2264	0.1281	0.1881	0.1581	0.1561	0.1018	0.1584	0.1697
	PSN [1]	0.3221	0.2127	0.1887	0.1682	0.1509	0.1735	0.1458	0.2226
	sliding PSN [1]	0.1988	0.2042	0.1394	0.2653	0.1551	0.0827	0.1888	0.1900
	DSN (Ours)	0.1384	0.1420	0.1404	0.1349	0.1240	0.0362	0.0973	0.1324

Appendix B.7. Approximation Experiment

Dynamic decay adaptively retains part of historical information stored in the membrane potential based on changing input. From the perspective of approximation, dynamic decay is powerful to simulate the behaviors of spiking neurons with various internal structures. During training, the spiking neuron learns to construct different reset mechanisms to model different input by regulating decay. For example, if the information is better suited to be encoded in the form of hard reset, the spiking neuron only needs to approximate a binary classifier to decide whether to set α_t to be constant β or 0. This plasticity of dynamics potentially breeds rich memory abilities. To verify the expressiveness of spiking neurons with dynamic decay, we design an experiment of using dynamic decay to approximate the behaviors of multiple LIF neurons with hard or soft reset.

Overview. To begin with, we manually construct two distinct datasets with a timestep of $T = 128$ named A and B, and split them into training and test set. Dataset A has input signals following a normal distribution with parameters (μ, σ^2) , while dataset B is a collection of more regular signals including sine functions, sigmoid functions, step functions and Poisson encoding with different parameters. Afterwards, these signals are input into 6 LIF neurons with different reset mechanisms and membrane time constants. Then, we apply dynamic decay across $C = 6$ channels with the same input signals to approximate the membrane potential with that of the LIF neurons described above, using the Mean Squared Error (MSE) loss function. Lastly, we calculate the spike firing accuracy of the test set as evaluation metric.

Datasets. The normal distribution parameters of Dataset A are $\mu = 1, \sigma = 2$. A total of 11,000 samples are collected, with a training-to-test ratio

of 10 : 1. The signal generation methods of Dataset B is shown in Table B.14. Each type of signal generates 200 samples (totally 800 samples), with 10% randomly selected as test set and the remaining samples used for training.

Table B.14: The signal generation methods of Dataset B. $x = 0, 1, \dots, T - 1$. The notation $[a : b : c]$ means selecting c evenly spaced values from a to b . For example, $[5 : 15 : 5]$ is equal to 5, 7.5, 10, 12.5, 15. Different parameters can be combined with each other to obtain samples with different characteristics, with the corresponding c multiplied. For Poisson Encoding, $\text{Random}(\cdot)$ denotes the random sampling of a floating-point number from the interval $[0, 1]$, and each set of parameters is repeated 8 times to generate 8 samples.

Signal Type	Formulation	Specification
Sine Function	$\text{input} = A \sin(\omega x) + B$	$\omega = 2\pi \frac{C-1}{T-1}, A = [-2 : 3 : 5], B = [-2 : 3 : 8], C = [5 : 15 : 5]$
Sigmoid Function	$\text{input} = A \cdot \text{Sigmoid}(x')$	$x' = \frac{20}{T-1}x - 10 + B, A = [-2 : 5 : 10], B = [10 : 10 : 20]$
Step Function	$\text{input} = A \cdot \text{Heaviside}(x')$	$x' = x - B, A = [-2 : 5 : 10], B = [0 : T : 20]$
Poisson Encoding	$\text{input} = A \cdot \text{Heaviside}(p)$	$p = \text{Random}(x) - p_0, A = [-1 : 5 : 5], p_0 = [0.3 : 1 : 5]$

Spiking Neurons. We set the threshold of LIF neurons to be 1, and the structure of dynamic decay is as follows:

$$\mathbf{X}'_t = \text{CausalConv1D}_{\text{up}}(\mathbf{X}_{t-k+1:t}) \quad (\text{B.3})$$

$$\mathbf{X}''_t = \text{ReLU}(\mathbf{X}') \quad (\text{B.4})$$

$$\mathbf{X}'''_t = \text{CausalConv1D}_{\text{down}}(\mathbf{X}''_{t-k+1:t}) \quad (\text{B.5})$$

$$\boldsymbol{\alpha}_t = \text{Sigmoid}(\mathbf{X}'''_t)^{1/\tau} \quad (\text{B.6})$$

Here, $\mathbf{X}_t \in \mathbb{R}^{C \times 1}$, and $\mathbf{X}_{t-k+1:t}$ denotes k inputs from \mathbf{X}_{t-k+1} to \mathbf{X}_t . The function $\text{CausalConv1D}(\cdot)$ is causal 1D convolution and the indices up and down represent the expansion of the input channels from C to eC , and the reduction from eC to C , respectively. τ is a hyperparameter to fine-tune $\boldsymbol{\alpha}_t$. In this experiment, we set $k = e = 8$, and $\tau = 0.5$.

Training. We set a batch size of 128 and employ Adam optimizer [97] with a cosine decay schedule whose peak learning rate is 1×10^{-2} . The training epochs are 100. To align with the techniques used in the main text, we also conducted experiments using dynamic decay to approximate integer-valued spikes (we set $N = 4$). Since integer-valued spikes are only meaningful in the case of soft reset [65], we fit only LIF neurons with soft reset in this case.

Results and Discussions. Results in Table B.15 and Fig. B.7 show that dynamic decay generally fits well to LIF neurons with different reset structures under various types of input signals, indicating its potential for expressiveness.

When the spikes become integers, the fitting accuracy of dynamic decay further improves on both datasets, supporting our view that the integer-valued training technique and dynamic decay have a complementary effect in terms of expressiveness. Specifically, there are two details that merit our attention:

- As the membrane time constant increases, the fitting accuracy declines. This could be due to the growing influence of historical information on the integration mechanism of the spiking neuron, and modeling such information has always been a challenging task. However, in the current modeling of the LIF model, the value of τ_m typically does not exceed the range specified in Table B.15 (usually $\tau_m = 2$ in [13, 65]), and our focus is on more general fitting scenarios. Additionally, the introduction of integer-valued spikes can significantly suppress this fitting error.
- When the membrane potential approaches the threshold, the error between the membrane potential predicted by dynamic decay and the true value generated by the LIF neuron is small for noise that follows a normal distribution. However, for a sine wave signal, the error between the two is larger (see Fig. B.7). We speculate that the cause of this difference lies in the fact that the proportion of data near the threshold is smaller for the sine signal compared to the noise signal with a mean μ equal to the threshold. This makes it more difficult for dynamic decay to learn how to handle membrane potential fluctuations near the threshold.

Table B.15: Experimental results of applying dynamic decay to approximate various LIF neurons with reset mechanisms on manually constructed datasets with different signals. Each channel of the parallel spiking neuron with dynamic decay is fitted with a LIF neuron. We report the spike firing accuracy (%) across 6 different channels and average them. *: results with integer-valued spike.

Channel	LIF neurons to fit	Dataset A	Dataset B	Dataset A*	Dataset B*
1	hard reset, $\tau_m = 4/3$	99.49	98.36	—	—
2	hard reset, $\tau_m = 2$	95.10	95.50	—	—
3	hard reset, $\tau_m = 4$	85.87	90.18	—	—
4	soft reset, $\tau_m = 4/3$	99.03	98.20	99.30	99.01
5	soft reset, $\tau_m = 2$	93.87	96.40	98.50	98.14
6	soft reset, $\tau_m = 4$	84.83	91.65	97.59	97.82
Average	—	92.97	95.05	98.46	98.32

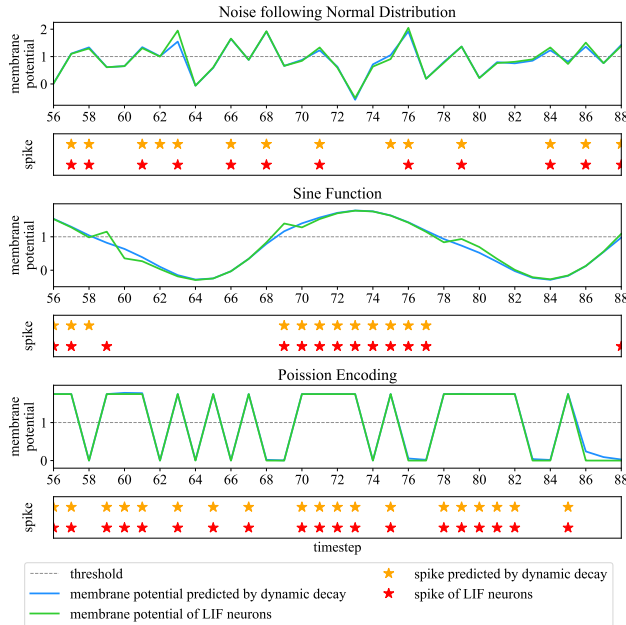


Figure B.7: Signal responses including membrane potential and spike for LIF neuron and its dynamic decay prediction on channel 2. Subplots from top to bottom depict the responses to a noise following normal distribution, sine function, and Poisson encoding.